Chapter 12
Simulating the Effects of Nutrient Loading Rates and Hypoxia on Bay Anchovy in Chesapeake Bay Using Coupled Hydrodynamic, Water Quality, and Individual-Based Fish Models

Aaron T. Adamack, Kenneth A. Rose and Carl F. Cerco

Abstract Water quality in the Chesapeake Bay has decreased since the 1950s due to an increase in nutrient loadings that have increased the extent and duration of hypoxic conditions. Restoration via large-scale reductions in nutrient loadings is now underway. How reducing nutrient loadings will affect water quality is well predicted; however, the effects of reduced nutrients (reduced food availability) and associated reduced hypoxia on fish are generally unknown as most water quality models do not include trophic levels higher than zooplankton. We dynamically coupled a spatially explicit, individual-based population dynamics model of juvenile and adult anchovy to the three-dimensional Chesapeake Bay eutrophication model. Growth rates of individual anchovy were calculated using a bioenergetics equation. Anchovy consumption rates were forced by zooplankton densities from the water quality model, and anchovy consumption of zooplankton was added as an additional mortality term on zooplankton in the eutrophication model. Anchovy mortality was size dependent and their movement depended on water temperature, dissolved oxygen, and zooplankton concentrations. Multi-year simulations with fixed annual recruitment were performed under decreased, baseline, and increased nutrient loadings scenarios. The results of our analyses show that anchovy

A.T. Adamack (✉) · K.A. Rose
Department of Oceanography and Coastal Sciences, Louisiana State University,
Energy, Coast, and Environment Building, Baton Rouge, LA, USA
e-mail: aaron.adamack@gmail.com

K.A. Rose
e-mail: karose@lsu.edu

C.F. Cerco
U.S. Army Engineer Research and Development Center, Vicksburg, MS, USA
e-mail: carl.f.cerco@usace.army.mil

Present Address:
A.T. Adamack
Institute for Applied Ecology, University of Canberra, Bruce, ACT, Australia

responses to changed nutrient loadings are dominated by changes in productivity, including simultaneous changes in growth and mortality rates, and spatial distribution, and depend on life stage. As such, we recommend using full life cycle, spatially explicit population models that are dynamically coupled to water quality models as a tool for predicting the effects of changes in nutrient loadings on fish population dynamics.

Keywords Nutrient loading · Hypoxia · Bay anchovy · Numerical modeling · Population dynamics · Individual-based model · Chesapeake Bay

12.1 Introduction

Understanding the link between water quality and fish population dynamics is especially important with the widespread efforts, often at considerable cost, to reduce eutrophication in coastal waters (e.g., Cloern 2001; Rabalais et al. 2002; Breitburg et al. 2003; Conley et al. 2009). Changes in how an ecosystem is managed, such as altering the rates of nutrient loadings, can have large and complex impacts on the ecosystem (Rabalais et al. 2002) including changes in the timing and spacing of ecosystem production dynamics. Historically, water quality models (freshwater) and nitrogen–phytoplankton–zooplankton (marine) models simulated the lower trophic level food web in order to predict chlorophyll-a and nutrient cycling (Rose et al. 2017). Zooplankton were included to get a realistic mortality term for the phytoplankton (i.e., closure term), and predicting realistic temporal and spatial variation in the zooplankton biomasses was a second-order consideration (Runge et al. 2004, Lett et al. 2009). Distinct from these models were the extensive efforts to simulate upper trophic level population dynamics (e.g., fish population) and food web dynamics (e.g., Ecopath with Ecosim, Christensen and Walters 2004). Many fish growth and population models focus on fish dynamics and do not include water quality and trophic levels lower than zooplankton (e.g., Luo and Brandt 1993; Rose et al. 1999; Lett et al. 2009).

Assessment of the effects of nutrient loadings on fish population dynamics is complicated by not only increasing nutrients stimulating the lower trophic level food web (potentially more food for fish), but also triggering hypoxia (dissolved oxygen (DO) < 2 mg L^{-1}) that has potentially negative effects on fish growth, reproduction, survival, and distribution (Rose et al. 2009). Earlier modeling studies (Brandt and Mason 2003; Breitburg et al. 2003; Adamack et al. 2012) that linked output from a water quality model for the Patuxent River to models of fish populations showed that the responses of populations to the changes in nutrient loading rates can be complex and different across life stages. Quantifying the effects of low DO at the population level further complicates the analysis because most effects beyond individuals are likely indirect as a result of shifts in other species (prey and predators of the fish of interest) or arise from spatial displacement of the species to areas of lower habitat quality.

The need to link fish bioenergetics and population models with water quality is particularly important in the Chesapeake Bay (Bay) ecosystem. Historically, episodic hypoxia and anoxia occurred in deeper portions of the water column of the Chesapeake Bay (Cooper and Brush 1991; Cronin and Vann 2003; Hagy et al. 2004). Since precolonial times, total nitrogen and total phosphorus loadings to the Bay are estimated to have increased 6.2-fold and 17.1-fold, respectively (Boynton et al. 1995), with much of the increase having occurred over the last century (Hagy et al. 2004; Kemp et al. 2005; Fisher et al. 2006); bottom-water hypoxia is now a persistent, annual occurrence. Nutrient loadings have increased because of a three-fold increase in human population size within the Bay watershed over the past 100 years, changing land-use patterns (initially forested, followed by large-scale clearing for agriculture, today agricultural lands are decreasing as land becomes urbanized or reverts to forests), and an increase in the use of agricultural fertilizers with the use of nitrogen-based fertilizer in Maryland doubling between 1960 and 2000 (Kemp et al. 2005). The Bay watershed is now undergoing a costly, multi-decadal restoration effort (Chesapeake Bay Program 2013) and had a total maximum daily load (TMDL) implemented for nutrients and sediments by the US Environmental Protection Agency in 2010 (US EPA 2010). The objective of the restoration program is to "Correct the nutrient- and sediment-related problems in the Chesapeake Bay and its tidal tributaries sufficiently to remove the Bay and the tidal portions of its tributaries from the list of impaired waters under the Clean Water Act." The cost of this plan has been estimated as 13–15 billion dollars to Maryland alone (Gray 2013). Quantification of the benefits of achieving these nutrient reduction goals to fish and the food web at the population and higher levels was recognized early on as a challenge (Kemp et al. 2005) that continues on to today.

Bay anchovy (*Anchoa mitchilli*) in Chesapeake Bay is a well-studied species (e.g., Houde et al. 1989; Houde and Zastrow 1991; Jung and Houde 2004a) that is a good candidate species for linking water quality to fish growth and population dynamics. Bay anchovy are one of the dominant fish species in the Bay in terms of both abundance and biomass (Baird and Ulanowicz 1989; Houde et al. 1989; Jung and Houde 2003), and bay anchovy are a major trophic link between zooplankton and piscivores (Baird and Ulanowicz 1989; Hartman and Brandt 1995). Bay anchovy consume 15–18% of zooplankton production during the summer and fall (70–90% of all zooplankton consumed by planktivorous fish), and in turn, they are the source of 60–90% of the energy intake of the piscivorous fish that fed upon bay anchovy during the summer, fall, and spring seasons.

Here, we dynamically couple a version of the three-dimensional Chesapeake Bay water quality model (Cerco and Cole 1993) with a spatially explicit individual-based population dynamics model for bay anchovy. The individual-based anchovy model simulates the growth, mortality, and spatial distribution of anchovy on the same three-dimensional spatial grid as the water quality model. The coupled models are used to predict the effects of increasing and decreasing the nutrient loadings to Chesapeake Bay on bay anchovy growth, biomass, and spatial distribution. We performed simulations for low and high levels of bay anchovy recruitment and for wet, normal, and dry water years. Additional simulations were performed to

examine how increased mortality during the egg and larval stages from exposure to hypoxia and how increased mortality rates on juveniles and adults due to increased habitat overlap of anchovy and their predators would affect the results.

12.2 Methods

12.2.1 Chesapeake Bay Water Quality Model

The Chesapeake Bay Environmental Modeling Package (CBEMP) was developed more than 20 years ago to assist in the management of eutrophication in the Chesapeake Bay ecosystem. The CBEMP has undergone continuous revisions and additions since then to respond to evolving management needs in the Chesapeake. Most recently, the CBEMP provided technical support for the development of the Chesapeake Bay TMDL (Batiuk et al. 2013). The CBEMP is comprised of three models: a three-dimensional hydrodynamics (CH3D-WES) model (Kim 2013), an eutrophication (CE-QUAL-ICM) model (Cerco et al. 2010), and a sediment diagenesis model (DiToro 2001).

   The most recent version of the CBEMP operates on a three-dimensional grid of 50,000 elements and simulates the period from 1985 to 2005 (Cerco and Noel 2013). These levels of spatial detail and temporal extent are in contrast to the original 4,073 cell grid and 1984–1986 simulation period used here. The original grid and application period are retained, however, for educational purposes and as a "test bed" for model development. The model code for this smaller grid has been updated to keep track with current developments made to the most recent finer resolution grid version. In this analysis, we used the original grid version for the 1984–1986 time period as the simpler model grid was more amenable to carrying out the model development process (e.g., modifying the water quality model code and testing model behavior after the addition of fish), the necessary input model runs were readily available, and it sufficiently captured the major dynamics needed for linkage to fish with quicker run times. The initial application of the version of the CBEMP used here for the years 1984–1986 was described by Cerco and Cole (1993).

   For the original grid (4,073 cell grid which we used here), the Bay's surface was divided into a horizontal grid of 729 cells with horizontal side lengths of ∼5 by 10 km (Fig. 12.1). Vertically, each column of cells is 2–15 cell layers (each cell is about 1.5 m thick) deep. The hydrodynamics model is run separately from the eutrophication and diagenesis models and employs curvilinear coordinates in the surface plane and a Z-grid in the vertical direction to produce three-dimensional predictions of velocity, diffusion, surface elevation, salinity, and temperature for each cell on an intra-tidal (about 5 min) timescale. Outputs from the hydrodynamics model that were used in the water quality model include cell volume, flows between cells in the axial, transverse, and vertical directions, and vertical turbulent diffusion. A Lagrangian processor was used to filter out intra-tidal details from the
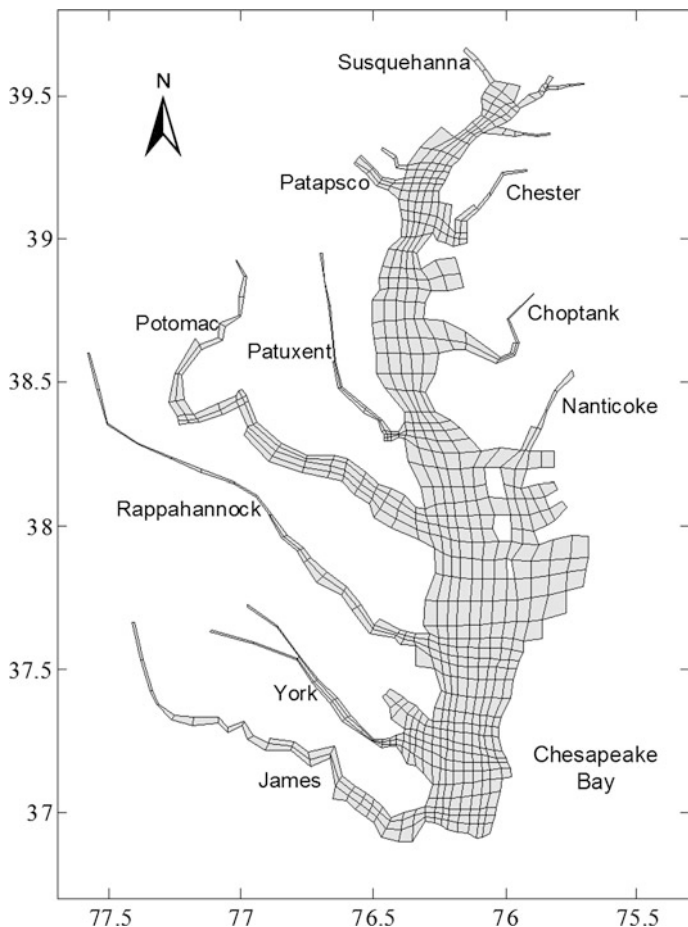
Fig. 12.1 Chesapeake Bay water quality model grid and the location of some key tributaries

hydrodynamic output, while maintaining the intertidal scale (about 12 h) transport (Dortch et al. 1992). Inputs to the hydrodynamics model include wind speed, air temperature, tributary freshwater inflows, surface heat exchange, tides, and the time-varying vertical distributions of temperature and salinity at the open boundary. Calibration and validation of the original model are described by Johnson et al. (1993).

The eutrophication and diagenesis models are run simultaneously. The eutrophication model simulates the nutrient, phytoplankton, and zooplankton dynamics in Chesapeake Bay on the same three-dimensional model grid as the hydrodynamics model (Kim 2013). Additionally, the eutrophication model provides boundary conditions in the water column including dissolved oxygen, temperature, and nutrient concentration, for the sediment diagenesis model (DiToro 2001). The

diagenesis model computes sediment-water fluxes of nitrate, ammonium, phosphate, dissolved oxygen, and silica based on these boundary conditions and on computed particle deposition. The concentrations of 23 constituents are tracked in the eutrophication and diagenesis models, including temperature, salinity, DO, several forms of dissolved and particulate carbon, nitrogen, and phosphorus, summer and winter phytoplankton groups, and micro- and mesozooplankton biomasses. The primary forcing functions for the eutrophication model were transport information from the hydrodynamic model, fall-line nutrient loads from the Susquehanna River and other major tributaries, non-point-source loads from below the fall line, point-source loads from municipal and industrial sources, atmospheric loads, open-mouth boundary conditions, solar radiation, and meteorological conditions (Cerco et al. 2010).

Model constituents were computed on a mass/unit volume basis in each cell on the three-dimensional computational grid. Biological constituents, including phytoplankton and zooplankton, were quantified as carbonaceous biomass. Constituent dynamics were updated approximately every 15 min for each model cell using a three-dimensional mass-conservation equation that was solved using the finite-difference method.

In addition to improvements and enhancements to the hydrodynamics and eutrophication models since the original version used here, another significant development has been the addition of living resources to the model. These living resources include bivalve filter feeders (Cerco and Noel 2007, 2010) and vertebrate species such as Atlantic menhaden (Dalyander and Cerco 2010). Indeed, the anchovy analysis described here inspired the subsequent development of the menhaden addition to the recent version of the hydrodynamics–eutrophication model.

12.2.2   Bay Anchovy Model

The bay anchovy model is a spatially explicit individual-based population model (IBM) that tracks the growth, mortality, and movement of individual anchovy in the same three-dimensional grid as the hydrodynamics and eutrophication models. The anchovy model was inserted directly into the eutrophication model code so that it operates on the same time steps as the eutrophication model and is able to directly interact with the eutrophication model. Anchovy consumption rates are dependent on the micro- and mesozooplankton densities and temperature generated by the eutrophication model for each cell and time step, bioenergetics (respiration and egestion) are dependent on temperature, horizontal movement of anchovies is related to zooplankton densities and temperature, vertical movement depends on temperature and DO, and growth and mortality are affected by low DO. Zooplankton biomass consumed by the anchovy is returned to the eutrophication model in the form of particulate and dissolved nutrients. Parameter values and a brief description of parameters for anchovy bioenergetics and movement are shown in Table 12.1.

Table 12.1 Parameter values used in the model equations for bay anchovy growth and consumption from Luo and Brandt (1993) and for the bay anchovy kinesis movement model. Values of the eight K feeding efficiency parameters were determined during calibration of the model. Values of the vulnerability parameters (v) were all set to one and so did not affect the proportion of micro- versus mesozooplankton consumed

Symbol	Description	Value
Consumption		
a_c	Intercept for maximum consumption (g prey (g wet weight)$^{-1}$ d^{-1})	0.41
b_c	Exponent for maximum consumption	−0.33
Q	Slope for temperature dependence on consumption	2.22
T_o	Optimum temperature for consumption (°C)	27
T_m	Maximum temperature for consumption (°C)	33
K_{11}	Half saturation for microzooplankton for anchovy < 43 mm (g wet weight m^{-3})	4.8
K_{12}	Half saturation for mesozooplankton for anchovy < 43 mm (g wet weight m^{-3})	0.04
K_{21}	Half saturation for microzooplankton for anchovy 43–60 mm (g wet weight m^{-3})	10.0
K_{22}	Half saturation for mesozooplankton for anchovy 43–60 mm (g wet weight m^{-3})	2.0
K_{31}	Half saturation for microzooplankton for anchovy 60–90 mm (g wet weight m^{-3})	20.0
K_{32}	Half saturation for mesozooplankton for anchovy 60–90 mm (g wet weight m^{-3})	5.0
K_{41}	Half saturation for microzooplankton for anchovy > 90 mm (g wet weight m^{-3})	80.0
K_{42}	Half saturation for mesozooplankton for anchovy > 90 mm (g wet weight m^{-3})	20.0
v_1	Vulnerability of microzooplankton to anchovy	1.0
v_2	Vulnerability of mesozooplankton to anchovy	1.0
Respiration		
a_r	Intercept for maximum standard respiration (g O$_2$ (g wet weight)$^{-1}$ d^{-1})	0.0115
b_r	Exponent for maximum standard respiration	−0.346
Q_r	Slope for temperature dependence of standard respiration	2.25
T_{or}	Temperature for standard respiration (°C)	30
T_{mr}	Maximum temperature for standard respiration (°C)	36
S	Specific dynamic action coefficient	0.10
A_c	Activity parameter	2.0
Egestion and excretion		
A	Intercept for temperature dependence of egestion	0.77
B	Exponent for temperature dependence of egestion	−0.40
a_u	Proportion of assimilated food excreted	0.15
Caloric density		
Cal_z	Caloric density of micro- and mesozooplankton (calorie (g prey)$^{-1}$)	610

(continued)

Table 12.1 (continued)

Symbol	Description	Value
Cal_F	Caloric density of bay anchovy (calorie (g wet weight)$^{-1}$)	1000
Mortality		
q	Multiplier of length-dependent mortality rate	1.17
Movement		
H_1	Height parameter for the inertia component of movement	0.75
H_2	Height parameter for the random component of movement	0.9
Φ	Maximum swimming velocity (BL s^{-1})	1.0
Q_{M0}	optimum temperature for horizontal (°C)	27
σ	standard deviation of temperature for horizontal (°C)	2
Q_{M0}	prey availability (fraction of C_{MAX}) for horizontal	0.8
σ	standard deviation of prey availability for horizontal	0.05
Q_{M0}	optimum temperature for vertical (°C)	27
σ	standard deviation of temperature for vertical (°C)	4
Q_{M0}	optimum dissolved oxygen (mg L^{-1}) for vertical	5.0
σ	standard deviation of dissolved oxygen (mg L^{-1}) for vertical	1.5

In order to conveniently track the movement of individual anchovy, the grid coordinates were converted from the latitude and longitude coordinates used in the eutrophication model to Universal Transverse Mercator (UTM) coordinates, which are given in terms of meters (m). The conversion was done using the equations of Snyder (1987) and assumed that the shape of the Earth conformed to the dimensions assumed by the 1980 Geodetic Reference System/World Geodetic System 1984 ellipsoid. To confirm that model cell sizes were consistent for the two grids, the horizontal side lengths of the anchovy model grid cells were compared to the eutrophication model grid cells. Differences in side lengths for the two grids are less than 0.1 m per side.

12.2.2.1   Annual Recruitment of Juveniles

A fixed number (low, median, or high) of 23 mm long, 30-day-old bay anchovy were added to the model each year as weekly cohorts for the duration of the simulation. There are about 10^9 to 10^{14} bay anchovy individuals in Chesapeake Bay (Jung and Houde 2004a), and modeling each individual separately is not possible computationally. To solve this, we used a super-individual approach (Scheffer et al. 1995). Each super-individual being simulated was given an initial worth, the number of identical population individuals that each super-individual represented.

The initial worth of each super-individual within a recruitment scenario was set to a constant value that was determined as the total number of 23 mm recruits being added in a simulation year divided by the number of super-individuals (about 10^5 super-individuals were used). The initial worth of each super-individual was

therefore 3.6×10^6 individuals for the low recruitment scenario, 1.2×10^7 individuals for the median recruitment scenario, and 1.584×10^7 individuals for the high recruitment scenario.

Use of super-individuals affected how anchovy mortality, consumption, and almost all model outputs were computed. In a true individual-based approach, the mortality rate would be converted to a probability of death and compared to a random number to determine whether the model individual was either removed or left in the population. Super-individuals remain in the simulation; mortality was simulated by decrementing the super-individual's worth by the total mortality rate (M_T, d^{-1}):

$$Worth_{i,t+1} = Worth_{i,t} e^{-M_T(\Delta t)} \qquad (12.1)$$

where $\Delta t = \sim 0.0104$ days (15/1440 min). When a super-individual reached old age (1095 days) or its worth dropped below 0.001, it was removed from the simulation. The total amount of prey consumed by a super-individual during a time step was determined by multiplying the amount of prey consumed by a single model individual by the super-individual's worth. Model predictions of anchovy densities, lengths, weights, and other outputs were weighted by the worth (in the statistical sense) of each super-individual. For example, a mean length on a given day was the weighted average of the lengths of the super-individuals, with the weights for averaging being the worths of the super-individuals when they were output.

The number of individuals added each week as part of annual recruitment had a triangular distribution with the smallest cohorts being added in early June and mid-October and the largest cohort being added in mid-August (Luo and Musick 1991; Zastrow et al. 1991; Jung and Houde 2004a). Newly generated super-individuals were randomly placed in model cells in the spatial grid that had DO concentrations greater than 3.0 mg L^{-1} and zooplankton concentration greater than 0.005 g C m^{-3}. The probability of a newly generated super-individual being placed in a particular cell was set to the volume of each cell as a proportion of the total volume of all 4,073 cells. If the minimum DO and zooplankton concentrations were not met, a new initial cell was randomly selected for the anchovy.

12.2.2.2   Growth and Bioenergetics

Growth of each individual was based upon the Luo and Brandt (1993) bay anchovy bioenergetics model and was evaluated each eutrophication model time step (every 15 min):

$$\frac{dW}{dt} = [CON - (R + SDA + F + E + REP)] \cdot \frac{Cal_z}{Cal_f} \cdot W \cdot f(DO_{cell}) \qquad (12.2)$$

where W is the wet weight (g wet weight) of an individual, CON is the amount of prey consumed, R is the respiration, SDA is the specific dynamic action, F is the

egestion, E is the excretion, REP is the reproduction, Cal_z is the caloric density of prey (cal (g prey)$^{-1}$), Cal_f is the caloric density of anchovy (cal (g wet weight)$^{-1}$), and $f(DO_{cell})$ is the low DO effect on growth. Consumption and the loss terms were all in units of g prey (g wet weight)$^{-1}$ d^{-1}. The ratio of the caloric densities converts g prey into g anchovy for the terms within the brackets to obtain the units of g anchovy per g anchovy per day.

The values of temperature and zooplankton densities that affected anchovy growth and consumption were those predicted for the cell currently occupied by an individual by the eutrophication model. Consumption was the sum of the amount of the microzooplankton and mesozooplankton consumed by an anchovy during each time step and depended on a maximum possible consumption rate and a type 2 functional response:

$$CON = \sum_{j=1}^{2} C_j \tag{12.3}$$

$$C_j = \frac{CON_{\max}(PD_j v_j / K_{cj})}{1 + \sum_{k=1}^{2} (PD_k v_k / K_{ck})} \tag{12.4}$$

where C_j is the consumption of prey type j by the individual anchovy, PD_j are the densities of microzooplankton (j = 1) and mesozooplankton (j = 2) in the cell of the individual, v_j is the vulnerability (all assumed 1.0), and K_{cj} are the half-saturation parameters based on size interval c of the anchovy. Zooplankton densities were converted from g C m^{-3} in the eutrophication model to g wet weight m^{-3} for use in the anchovy model by multiplying by 12.5 (dry weight was 20% of wet weight and carbon weight was 40% of dry weight; Mauchline 1998). Maximum consumption rate was an allometric function of anchovy weight and temperature:

$$CON_{\max} = a_c W^{b_c} \cdot f(T) \tag{12.5}$$

where a_c and b_c determine the weight effect; $f(T)$ is bell-shaped function that is one at the optimum temperature, T_o; zero at the upper temperature, T_m; and Q is a parameter that approximates a Q_{10} relationship (a measure of the change in biological rates as a consequence of increasing temperature by 10 °C) within the $CON_{\max}$ function for temperatures below T_0.

Respiration was modeled as a power function of weight and then adjusted for temperature using the same temperature effect function as with CON_{max} but with different parameter values for the optimum and upper temperatures and for the Q_{10} relationship:

$$R = a_r W^{b_r} f(T) A_c \tag{12.6}$$

where a_r and b_r determine the weight effect; T_{or}, T_{mr}, and Q_r are specified for f (T) for respiration; and A_c is the activity multiplier. The values of T_{or} and T_{mr} were set so that respiration rate increased over the range of simulated temperatures.

Egestion was represented as a fraction of consumption, while excretion and specific dynamic were represented as fractions of assimilated energy (consumption minus egestion).

$$F = CON \cdot A \cdot T^B \tag{12.7}$$

$$E = (CON - F) \cdot a_u \tag{12.8}$$

$$SDA = (CON - F) \cdot S \tag{12.9}$$

where A and B determine the temperature effect on egestion, a_u is the fraction of assimilated energy lost to excretion, and S is the fraction of assimilated energy lost to specific dynamic action.

Energy related to reproduction (REP in Eq. 12.2) was computed as the grams/day expended during days 115–246 of each year by anchovy that were at least 43 mm long and that had a positive net energy intake for the time step. The energy used for reproduction was set to half of the net energy intake, and reproduction costs were applied to all individuals (males and females).

A logistic sigmoidal function, developed originally by Luo et al. (2001) for Atlantic menhaden, was used to simulate the physiological effects of exposure to low dissolved oxygen on anchovy growth rate.

$$f(DO_{cell}) = 1/(1 + e^{(-2.1972 DO_{cell} + 6.5916)}) \tag{12.10}$$

The function $f(DO_i)$ used the DO in the cell to determine the multiplier, and then the multiplier was applied to the predicted change in weight of the anchovy for that time step (Eq. 12.2). Growth begins to be reduced at a DO of about 6 mg L^{-1} is 50% of normal growth at 3 mg L^{-1} and approaches zero at DO concentrations less than 1 mg L^{-1}.

Anchovy weights were converted into lengths using a weight–length relationship modified from Jung and Houde 2004a:

$$L_{new} = \left(\frac{W}{e^{-11.799}}\right)^{\frac{1}{3}} \tag{12.11}$$

where L_{new} is the new length of the anchovy and $e^{-11.799}$ is a constant derived from a length–weight function fitted to summer (July) anchovy lengths and weights. An anchovy's length only changes if its new length is longer than its length during the previous time step.

12.2.2.3 Mortality

Four sources of mortality were included in the bay anchovy model: general mortality (M_G), starvation mortality (M_{starv}), mortality due to exposure to low DO (M_{DO}), and mortality due to old age. Once each 15-min time step, the general, DO-related, and starvation mortality rates were summed to get total mortality (M_T), and used to update the worth of the super-individual (Eq. 12.1). Old age mortality was threshold based on age (i.e., not a rate) and resulted in the elimination of the super-individual with all of its worth.

General mortality represented all causes of anchovy mortality except mortality due to low DO, starvation, and old age. The rate was a simple constant during winter (October through March) and decreased with anchovy length during the summer (April through September).

$$M_G = q \cdot L^{-1} \tag{12.12}$$

where q is the multiplier for length-dependent mortality. Jung and Houde (2004a) estimated wintertime and length-dependent summer mortality rates based upon 6 years (1995–2000) of field data. As low DO, starvation, and old age mortality are added to the general rate in the model, we used the lowest summer ($q = 1.17$) and winter mortality rates (0.005 d^{-1}) estimated by Jung and Houde (2004a) for general mortality.

Mortality rate due to exposure to hypoxia was a function of the DO concentration in the cell.

$$M_{DO} = 0.093487 + 70.11894 \cdot (\ln[\text{DO}_{\text{cell}}])^2 \tag{12.13}$$

This function was fit to experimental data on Atlantic menhaden (*Brevoortia tyrannus*) reported by Burton et al. (1980). As observed mortality rates become extremely high at low DO concentrations, and as anchovy only moved vertically once every 4 eutrophication model time steps (each eutrophication model time step simulates ~15 min of real time; 4 eutrophication model time steps ≈ 1 h of real time), the maximum mortality rate due to exposure to very low DO was set to a very high value (33.78 d^{-1}). This high mortality rate resulted in almost complete mortality for the super-individual after 4 time steps, and thus, if such long exposure occurred, the individual would be removed from the simulation due to near zero worth.

Starvation mortality (0.1 d^{-1}) was applied to anchovy model individuals whose weight was 70% or less of the expected weight given their length for each time step that an anchovy was below its expected weight. Mortality due to old age (100% mortality; super-individual removed from simulation) was applied to all model individuals upon reaching an age of 1,095 days (3 years old) based on Newberger et al. (1989), who found that bay anchovy generally did not live past 3 years of age.

12.2.2.4 Movement

A kinesis approach (Humston et al. 2000; Humston 2001; Watkins and Rose 2013) was used to simulate the horizontal and vertical movement of each anchovy super-individual. Anchovy positions were tracked in continuous x, y, and z space. The x and y coordinates corresponded to an individual's UTM coordinates, while the z coordinate was the distance from the water surface. Horizontal and vertical movements were evaluated separately at fixed time intervals (x and y every 12 h; z hourly) to improve model run time, to account for differences in the distances involved and the time required for an anchovy to cross model cells in the horizontal and vertical planes, and to allow for the establishment of an inertial gradient (described below). Horizontally, model cells are several kilometers across and could require more than a day for an adult anchovy (e.g., ~5 cm TL) to cross the cell if they took the most direct path across the cell. Vertically, model cells are only 1.5 meters and an adult anchovy could swim from the bottom of a cell to the top of the cell in ~30 s. The movement model added together an inertia component ($f(V_{t-1})$) and a random component ($g(\varepsilon)$) to produce a net velocity for each of the x, y, and z dimensions each time step.

$$V_t = f(V_{t-1}) + g(\varepsilon) \tag{12.14}$$

where $f(V_{t-1})$ is a function that was based upon the anchovy's velocity during the previous movement step, and g(ε) is a randomly generated velocity. The net velocities were then multiplied by the time since the last movement step to determine changes in distance for x, y, and z, which then were added to the current location to get a new x, y, and z location and a cell location.

The relative contribution of inertial versus random components was dependent on how close a movement cue was to its optimum level. When conditions in a cell were close to the optimum, the inertial component dominated movement. When conditions in a cell were far from the optimum, the random component dominated movement. Both functions were described using Gaussian functions:

$$f(V_{t-1}) = V_{t-1} \times H_1 \left[e^{(-0.5)[(Q_M - Q_{M0})/\sigma]^2} \right] \tag{12.15}$$

$$g(\varepsilon) = \varepsilon \times H_2 \left[e^{(-0.5)[(Q_M - Q_{M0})/\sigma]^2} \right] \tag{12.16}$$

where H_1 and H_2 control the height of the function and were restricted to the range 0–1.0, σ controlled the width of the Gaussian function, ε is a random number deviate drawn from a normal distribution with a mean and standard deviation based on an individual's swimming speed, Q_M is the actual value of the movement cue, and Q_{M0} is the optimum value of the movement cue. For the two components of the movement model to work properly, model individuals needed to shift between cells somewhat frequently (in terms of movement steps) in order to generate cue gradients that will drive the inertia component of the movement model. As vertical

distances across cells were short, vertical movement could be evaluated frequently (hourly) while the relatively long horizontal distances across cells required longer movement time steps (12 h).

Horizontal (x and y) movement depended on the cues from water temperature and zooplankton density, while vertical (z) movement depended on water temperature and DO. Water temperature and prey availability were used as cues because they were the key factors affecting anchovy growth, while DO was used as a cue because it affects the vertical distribution of anchovy and other fish species (e.g., Constantini et al. 2008 and Zhang et al. 2009) and can cause direct mortality. The optimal water temperature (Q_{M0} for temperature) was set to 27 °C, the optimal temperature for consumption by anchovy (Luo and Brandt 1993). Densities of micro- and mesozooplankton were combined into a single measure of overall prey availability using the functional response portion of the equation for consumption, and the optimum value for prey availability (Q_{M0} for food) was set to 80% of CON_{MAX} (Eq. 12.5). To avoid mortality due to low DO, while at the same time preventing anchovy from aggregating at the surface of the water column, we set the optimum DO concentration (Q_{M0} for DO) to 5.0 mg L^{-1}.

Deviates from optimal were computed separately for each cue, and the smaller of the deviates for water temperature and prey availability was used to determine the net velocities for x and y movement, while the product of the deviates for water temperature and DO was used for vertical movement. Vertical movement was restricted to a maximum change of 3 m per vertical movement step in order to simplify the tracking of anchovy movement, as anchovy can potentially swim many times the thickness of the water column between the 1 h movement time steps.

Once the distances that an anchovy moved along x, y and z had been determined, a two-part procedure was used to update the anchovy's position. In the first part of the procedure, the anchovy's new x and y values were determined by adding the distances moved along the x and y coordinates to the anchovy's previous position. A point-in-polygon subroutine (Burkadt 2014) was used to determine whether the anchovy's new position was outside of the cell that it had begun the time step in. If the anchovy finished in the same cell that it started in, the anchovy's horizontal movement was complete for the current movement step. If the anchovy's new position was outside the initial cell, then the anchovy's position was checked to determine whether or not it was on the model grid for the current depth layer. If the individual's new position was not on the grid, then the individual was reflected back onto the grid. Finally, the individual's new cell was identified and updated.

The second part of the movement updating procedure was to update the individual's vertical position. Updating vertical position was simpler as z values were constrained to the interval between the surface and bottom of the water column, and all cells in the vertical dimension were in had the same shape and thickness. If the z value was above the surface or below the bottom, then the z value was reset to place the anchovy just below the surface or just above the bottom. Once the anchovy's final position was determined, its velocities along the x- and y-axes for the current movement step were recalculated using the anchovy's starting and actually realized final positions. The recalculated velocities were used to set V_{t-1} for the next movement step.

12.2.3 Modifications to the Eutrophication Model to Accommodate Bay Anchovy

The eutrophication model had been calibrated previously without anchovy predation on zooplankton. To accommodate the addition of anchovy to the eutrophication model, we reduced the mortality rates of summer algal biomass from 1.00 d^{-1} to 0.15 d^{-1}, and predation mortality on micro- and mesozooplankton by 70% based on model calibration results.

12.3 Simulations

Three sets of model simulations were performed: calibration and baseline to examine the effects of water year and recruitment level, effects of increased and decreased nutrient loadings, and the effects of forced increased mortality rates to offset the benefits of increased nutrient loadings (e.g., increases in zooplankton prey). The results of single model runs were reported, as runs that used different random number seeds generated very similar model predictions of anchovy growth, densities, and spatial distributions. We used eutrophication model input files and hydrodynamics output for the years 1984, 1985, and 1986; these were arranged to obtain a single 10-year sequence. The 3 years can be assigned water year types (e.g., normal, wet, and dry) by using the US Geological Survey (2014) classification of annual-mean stream-flow entering Chesapeake Bay: 1984 was a wet year, 1985 was a dry year, and 1986 was a normal year. Calibration runs used a repeating series of the input files for the 1986 conditions (normal years). For all other simulations, we linked the input files for the 1984 (wet), 1985 (dry), and 1986 (normal) water years in order to match the sequence of wet, normal, and dry water year types that were observed between 1984 and 1993 (Fig. 12.2). This was done to use a real sequence of water year types in model simulations. Settings for all of the model runs are summarized in Table 12.2.

12.3.1 Bay Anchovy Recruitment

Annual recruitment levels for the low and high recruitment scenarios were based on estimates of the total number of eggs produced each year by anchovy, and age-dependent growth and size-dependent mortality rates from Jung and Houde (2004a). The number of eggs produced was combined with growth and mortality rates to estimate the total number of 23 mm long bay anchovy (the initial size of anchovy added to the model; eggs and larvae were not directly included in our simulations) produced each year. Low (3.6×10^{11} individuals) and high (1.58×10^{12} individuals) recruitment levels were set to the years with the lowest
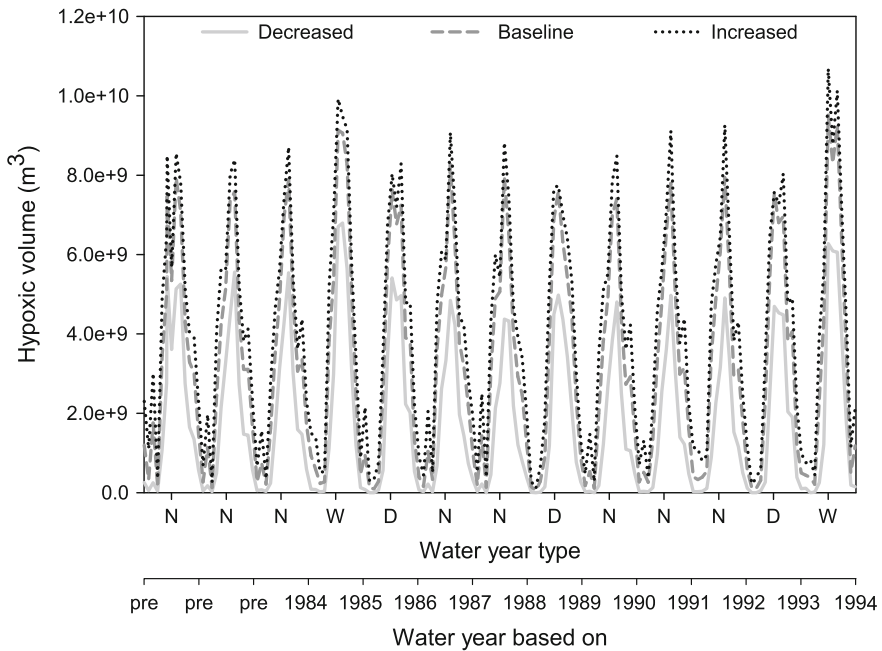
Fig. 12.2 Volume of hypoxic water for decreased, baseline, and increased nutrient loadings during the 3 prerun years and the 10 years after that used the same water year type as observed in 1984–1993. Spin-up years are indicated by the label "pre." Water year type is indicated by the initials: D = dry year, W = wet year, and N = normal year. Water year types were obtained from the USGS (http://www.md.water.usgs.gov/monthly/bay.html). Note that the calender year starts on the ticks for "Water year based on"

and highest numbers of 23 mm long individuals produced across the six annual estimates. Our low recruitment condition was probably truly low as data from the Maryland Department of Natural Resources Bay-wide index (2017) indicated that age-0 bay anchovy catch per unit effort has declined since 1959. Our high recruitment condition, while high for the 1995–2000 period, may be closer to average recruitment relative to the long-term record for anchovy in Chesapeake Bay.

12.3.2   Nutrient Loading Scenarios

Three nutrient loadings were used: baseline, decreased, and increased. The baseline nutrient loadings scenario used the nutrient loads estimated for the years 1984, 1985, and 1986. The decreased scenario reduced nutrient loads by 50% from baseline levels in each year. A 50% reduction in nutrient loadings was roughly equivalent to that required under the old Chesapeake 2000 Agreement, which required reductions of 48 and 53% (based on 1985 levels) for total nitrogen and

Table 12.2 Summary of the model runs analyzed in this paper. All simulations were structured 23 years long and started with 10 years of spin-up for nutrient loadings (no anchovy), then 3 years of spin-up for anchovy (normal water years), and then 10 years of water years that matched the water years of 1984–1993. The first 10 years for spin-up used all normal water years and the same nutrient loadings as was used for the 1984–1993 period. The 3 years of spin-up for anchovy also used normal water years and the low or high recruitment level used in 1984–1993

Run	Purpose	Nutrient loadings	Recruitment level	q in general mortality
1	Re-calibration and effects of water year and recruitment level	Baseline	Low	1.17
2		Baseline	High	1.17
3	Effects of increased and decreased nutrient loadings	Decreased	Low	1.17
4		Increased	Low	1.17
5		Decreased	High	1.17
6		Increased	High	1.17
7	Effects of decreased recruitment (increased egg or larval mortality) due to increased nutrient loadings	Increased	86% of Low	1.17
8		Increased	49% of Low	1.17
9		Increased	12% of Low	1.17
10		Increased	76% of High	1.17
11		Increased	52% of High	1.17
12		Increased	23% of High	1.17
13	Effects of increased general mortality rate of juveniles and adults due to increased nutrient loadings	Increased	Low	1.3
14		Increased	Low	1.43
15		Increased	High	1.3
16		Increased	High	1.43
17		Increased	High	2.3
18		Increased	High	2.725

phosphorus inputs (Kemp et al. 2005; Chesapeake Bay Program 2013). In the increased loadings scenario, nutrient loads are 50% higher than the baseline loads. The increased loadings scenario provides a contrasting scenario to the decreased loadings scenario. It may reflect future conditions if no action is taken, but no such land use and loadings projections have been made. Increases and decreases in nutrient loadings were applied through the use of a simple multiplier of the nutrient loading rates (e.g., nutrient loadings × 0.5 for the decreased nutrient loadings scenario and × 1.5 for the increased nutrient loadings scenario). In the standard 10-year simulations, the volume of hypoxic water was typically 20–40% less under decreased nutrient loadings and about 10–15% larger under increased nutrient loadings (Fig. 12.2). The model represents peak hypoxia in summer, coincident with peak primary production of organic matter and temperature-induced respiration. There can be some modeled residual hypoxia in isolated deep holes during winter. The residual hypoxia is an artifact of the relatively coarse grid and is absent in later, more highly resolved grids (e.g., Cerco and Noel 2013). The isolated persistent hypoxic volumes do not impact the anchovy, as the location and small spatial extent of any residual winter hypoxia did not affect anchovy habitat.

12.3.3   Initial Conditions from Spin-Up

All simulations were structured as 23-year simulations. Each simulation started with 10 years of spin-up for nutrient loadings (no anchovy), then 3 years of spin-up for anchovy (normal water years), and then 10 years of water years that matched the water years of 1984–1993. The first 10 years for spin-up used all normal water years and the same nutrient loadings scenarios as was used for the 1984–1993 period (e.g., 50% increase, baseline, or 50% decrease). The 3 years of spin-up for anchovy also used normal water years and the same low or high recruitment level as used in the 1984–1993 portion of the simulation. For example, run 13 (Table 12.2) had 10 years of no anchovy under normal water years and increased nutrient loadings, then 3 years with anchovy under normal water years, increased nutrient loadings and low recruitment, and then 1984–1993 water years under increased nutrient loadings, low recruitment, and q increased from 1.17 to 1.3.

12.3.4   Increased Mortality Rates

Changes in nutrient loadings can have several potential effects on bay anchovy that were not directly simulated in our bay anchovy model. Chesney and Houde (1989) used laboratory studies to show that anchovy egg hatchability declined significantly at DO concentrations less than 3 mg L^{-1}, while Adamack et al. (2012) used a simulation model and showed that increased spatial extent and duration of low DO conditions due to increases in nutrient loadings could result in significant increases in egg mortality rates. Costantini et al. (2008) and Ludsin et al. (2009) found that increases in the extent of hypoxia in Chesapeake Bay could increase the mortality rates of forage fish by increasing the degree of vertical spatial overlap between the forage fish and their predators resulting in increased encounter rates. The above studies were focused on the negative effects of increased hypoxia from increased nutrient loadings on anchovy. However, the reverse situation of decreased nutrient loadings reducing hypoxia resulting in less vertical spatial overlap between forage fish and their predators reducing their encounter rates and thereby reducing mortality is also possible and of potential importance.

To investigate those mortality-related effects not explicitly covered in the anchovy model, we ran two sets of simulations for the low and the high recruitment scenarios with increased nutrient loadings. The first set of simulations examined the potential effects of increased egg mortality due to increases in the vertical extent and intensity of hypoxia under the increased nutrient loadings scenario. The egg stage is not explicitly simulated in our model because we add recruits each year. We represented possible changes in egg (and larval) mortality rates by adjusting the recruitment levels. For the low and high recruitment scenarios, we tested three levels of recruitment reductions from the original recruitment levels with the goal of identifying how much larval recruitment had to be reduced in order to result in no

net gain in anchovy production relative to the baseline nutrient loading scenario. The minimum recruitment level tested for the low recruitment scenario was arbitrarily set to 12% of the baseline low recruitment level, while for the high recruitment scenario the minimum was set to the low recruitment level (23% of high recruitment). Two additional recruitment levels that were spaced evenly between the minimum recruitment level and the original recruitment level were tested for each recruitment scenario (low and high).

The second set of simulations examined the effects of increases in bay anchovy juvenile and adult mortality rate due to potential increases in the degree of vertical spatial overlap between anchovy and their predators. While we simulated anchovy vertical movement, predators were represented as a mortality rate. As an initial approach to simulating predator responses that would cause increased overlap, we increased q, the length-specific mortality coefficient (Eq. 12.12), from our original value of 1.17 to 1.3 and to 1.43. These values were the median and maximum values of q measured by Jung and Houde (2004a). The value of q was further increased to 1.725 and to 2.3, which were equivalent to instantaneous mortality rates that were about 50% and about 100% higher than the instantaneous mortality rates when q was set the baseline value of 1.17. These higher values of q were to ensure that mortality would be sufficiently high to offset the increased anchovy production under increased nutrient loadings.

12.3.5   Model Outputs

Model outputs are presented for the three sets of simulations: re-calibration and the baseline simulations, the effects of water years and nutrient loading on anchovy, and how changes in recruitment and mortality due to increased nutrient loads affect anchovy biomass. All model outputs and how they were computed from super-individuals in the simulations are documented in Table 12.3.

Results summarizing the baseline and re-calibration results include time series plots of daily total biomass, total abundance, and mean length, and comparisons of daily nutrient, chlorophyll-a, and micro- and mesozooplankton concentrations before and after the addition of anchovies to the model. We then summarize the baseline results using YOY individuals only in October from the last years (normal, dry, and wet) of the simulations: box plots of lengths, biomass, and abundance. Finally, we compared box plots of the latitudes of individuals between each water year type (last 3 years) and reported field data.

The effects of water year type and nutrient loadings also use mean length, biomass, and abundance for YOY in October. Two additional outputs are two-dimensional spatial maps of all individuals in July by water year type (last 3 years) and high or low recruitment, and the percentage of mortality due to the possible causes over all years in the simulations. The effects of additional mortality were assessed by comparing YOY biomass in October under increased loadings with various values of reduced recruitment and increased values of q to October

Table 12.3 Calculations performed to go from super-individuals to the model outputs reported in tables and figures in this paper

Model output	Calculations	Runs and Years	Figures
Daily biomass, abundance, and mean length of all individuals	Output all individuals on first time step of each day; compute summed weight x worth (biomass) and worths (abundance); compute mean length (weighted by worth)	Runs 1 and 2 All 13 years for each run	Figure 12.3
October YOY median length, growth rate, abundance, and biomass	Output all YOY individuals on first time step after midnight on October 15; compute the median length (weighted by worth), mean growth rate (weighted by worth) from 23 mm in length to current length of super-individual, summed worths (abundance), and summed weight x worths (biomass)	Runs 1 and 2 Last 3 years (dry, normal, and wet) of each run	Figure 12.4 (also Table 12.4)
Mean latitude in mid-October	Output all individuals on first time step after midnight on October 15; assign individuals to 10 mm size classes; compute box plots of latitudes (weighted by worth)	Run 2 Last 3 years (dry, normal, and wet) of the run	Figure 12.4
Box plot of lengths and biomass in mid-October, and percent survival (initial recruitment to October)	Output all YOY individuals on first time step after midnight on October 15; compute box plots of lengths (weighted by worth) and biomass (weights x worth); and compute survival as summed worths of all individuals on October 15 divided by initial total worth of 23 mm recruits	Runs 1–6 Last 3 years (dry, normal, and wet) of each run	Figure 12.5
Depth-integrated densities of age-1 and older anchovy	Output all age-1 and older individuals on first time step after midnight on July 15; compute summed worths of all individuals over depth by surface grid cell	Runs 3–6 Last 3 years (dry, normal, and wet) of each run	Figure 12.6
Mean latitude by month of age-1 and older individuals	Output the latitude and worth of each age-1 and older individual on midnight of the midpoint day in each of April, May, June, July, and August; compute the mean latitude (weighted by worth)	Runs 3–6 Last 3 years (dry, normal, and wet) of each run	Figure 12.7

(continued)

Table 12.3 (continued)

Model output	Calculations	Runs and Years	Figures
Proportion of total mortality due to each cause	Cumulative sum of all worths due to mortality, and by each mortality source (hypoxia, starvation, old age, and natural); compute the proportions as sum of deaths by source divided by total deaths	Runs 1–6 All 13 years for each run	Figure 12.8
YOY biomass in mid-October	Output all YOY individuals on first time step after midnight on October 15; compute biomass as summed weight × worths	Runs 7–18 Last 3 years (dry, normal, and wet) of each run	Figure 12.9

biomass predicted under baseline conditions. The patterns in the model results that rely on snapshot outputs in October were consistent across water years, regardless of day selected for outputting, but the magnitude of the individual model results varied across output days.

12.4   Results

12.4.1   Baseline Simulations

In the baseline simulations (Runs 1 and 2), total (all ages) anchovy biomass (Fig. 12.3a) and abundance (Fig. 12.3b) show repeating annual cycles that reflect the effects of recruitment level more than water year type. Under high recruitment, biomass initially increased rapidly each year as recruits were added to the population and then dropped very rapidly due to the rising biomass of anchovy rapidly reducing their prey causing slower growth and higher mortality rates relative to the low recruitment scenarios. While biomass and abundance were much higher under high recruitment compared to low recruitment, mean length was lower under high recruitment confirming a density-dependent effect of abundance on growth (Fig. 12.3c). Abundance under high recruitment (Fig. 12.3b) initially dropped in tandem with a drop in biomass each year (Fig. 12.3a), suggesting that slowed growth led to increased mortality. Under low recruitment, both biomass and abundance showed smoother increases as juveniles were added and decreases after that each year, and the lower predation pressure on their zooplankton prey resulted in faster growth and longer mean lengths (gray lines in Fig. 12.3).

Within each of the baseline simulations, the annual cycles of biomass, abundance, and mean length did not show large differences among the dry, normal, and wet water years (Fig. 12.3). Use of total population, which included all ages, acted
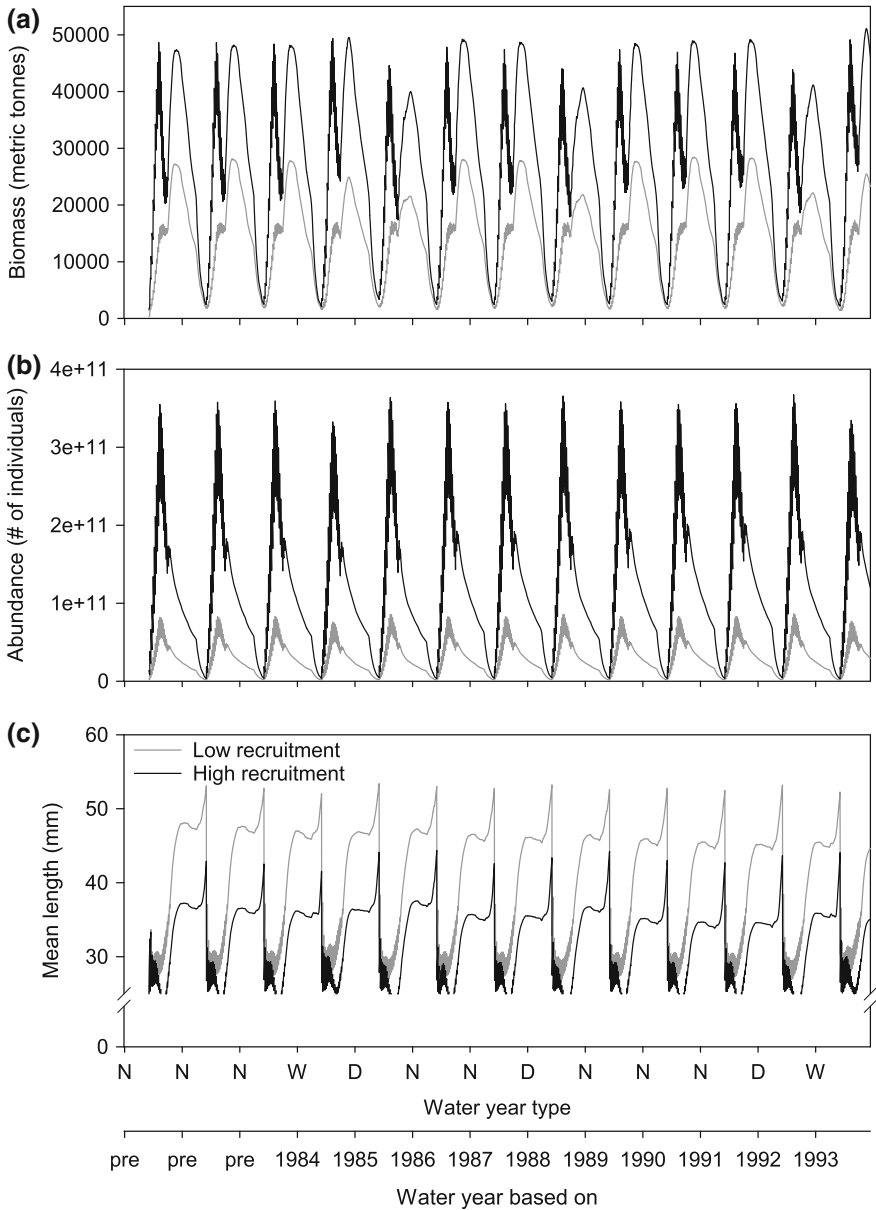
Fig. 12.3 Total daily population biomass (**a**), abundance (**b**), and mean length (**c**) for the baseline simulations under low and high recruitment

to smooth differences from year-to-year. When only YOY were examined, water year type had somewhat larger effects, but they were still small compared to the effects of recruitment level (discussed below in Fig. 12.6).

12.4.2 Assessment of Re-calibration Using Baseline Simulations

Following the re-calibration of the coupled models after adding bay anchovy, chlorophyll-a concentrations and mesozooplankton densities in the two simulations (Runs 1 and 2) were 1-fold to 3-fold higher than predicted values without anchovy. Predicted chlorophyll-a (based on the daily values) ranged from 0.85 to 18.65 g C m^3 with anchovy versus 0.67 to 14.10 g C m^3 without anchovy, and mesozooplankton ranged from 0.0037 to 0.12 g C m^3 with anchovy versus 0.0037 to 0.046 g C m^3 without anchovy. In contrast, microzooplankton densities ranged from a third of to being similar in magnitude to the predicted densities obtained without anchovy. The temporal and spatial trends in micro- and mesozooplankton densities were generally consistent with the densities from model runs without anchovy. Nitrate and phosphate concentrations were almost identical between simulations without and with anchovy. Adamack (2007) further demonstrated the similarity of micro- and mesozooplankton densities (with and without anchovy) to the historical field data (roughly monthly) collected at station CB5.2 from the long-term monitoring program (see Magnien 1987).

Model predictions of anchovy lengths and growth rates for YOY individuals that survived to the end of October for the baseline simulations (Runs 1 and 2) are somewhat comparable with the October field observations of Jung and Houde (2004a, their Table 2). The median length of anchovy under low recruitment was about 34 mm for all 3 water year types (last 3 years of the simulation), which is lower than the range of mean lengths (46.7–51.1 mm) reported by Jung and Houde (2004a). The shorter simulated lengths were driven by a combination of the date that model results were output and the pattern of recruitment that we used. Delaying output by 14 days resulted in median lengths being ∼5 mm longer, while ignoring recruits added in September and October produced additional increases in the simulated lengths. Simulated median lengths in the last 3 years of the high recruitment baseline simulation were about 27 mm, which is approximately half of the shortest mean lengths observed (46.7–51.1 mm, Table 12.4). Predicted YOY anchovy growth rates for both the low and high recruitment simulations (about 0.38 mm d^{-1}) are similar to Jung and Houde's values (0.36 and 0.40 mm d^{-1}), and also similar to the juvenile anchovy growth rates reported by others (0.20–0.33 mm d^{-1}) for mid-Chesapeake Bay (Morin and Houde 1989; Newberger et al. 1989).

Predicted abundances of YOY anchovy in late October for the two baseline runs are within the range of abundances observed by Jung and Houde (2004a) (Table 12.4). Anchovy abundances for the low recruitment scenario (44.4 to 48.4 × 10^9

Table 12.4 Predicted median length in October, mean growth rate of survivors, abundance, and biomass of YOY anchovy in dry, normal, and wet years of the baseline simulation under low and high anchovy recruitment compared to observed values from Jung and Houde (2004a). The years of field data are the lowest, median, and highest values of 23 mm anchovy recruits reported by Jung and Houde in order to provide a range of values to compare to the model results

Year type	Median length (mm)	Growth rate (mm d^{-1})	Abundance ($\times 10^9$)	Biomass (metric tonnes)
Low recruitment				
Dry	32.4	0.34	45.0	18,393
Normal	33.8	0.38	48.4	22,502
Wet	33.8	0.39	44.4	19,535
High recruitment				
Dry	26.1	0.15	169.1	28,346
Normal	27.3	0.14	187.6	39,094
Wet	28.3	0.14	177.9	39,684
Jung and Houde (2004a)				
Low (1996)	49.1	0.36	29.2	27,000
Median (1997 and 1999)	51.1	0.36	98.2	~100,000
High (1998)	46.7	0.40	273.8	193,000

individuals) are similar to the observed abundance in 1995 (44.5×10^9 individuals), which was the year with the second lowest observed YOY recruitment. Predicted abundances for the high recruitment scenario ($169.1–187.6 \times 10^9$ individuals) are between the median and highest levels of recruitment observed by Jung and Houde ($98.2–273.8 \times 10^9$ individuals).

October YOY biomass tended to be low relative to the October standing stock biomass of anchovy reported by Jung and Houde (Table 12.4). Anchovy biomasses predicted for low recruitment (18,393–22,502 metric tonnes) are similar to the fall peak in biomasses observed by Jung and Houde during years with low estimated anchovy biomass (~25,000–50,000 metric tonnes; their Fig. 4a). However, predicted biomasses for the high recruitment scenario (28,346–39,684 metric tonnes, Table 12.4) are less than half of the reported field-based estimates (~100,000–150,000 metric tonnes) during years with high anchovy biomass.

Model predictions of the mean latitude of age-1 and older anchovy (not YOY) by length category are generally comparable to field data from the CHESFIMS project (Miller et al. 2008). When each of the simulated water years were matched with field data for years of similar water type, the predicted mean latitude of anchovy overlaps with the observed latitudes for the intermediate length classes (Fig. 12.4)

We examined the vertical distributions of anchovy for two cross sections of Chesapeake Bay (not shown) and found that anchovy were generally concentrated in waters above the hypoxic layer, consistent with Zhang et al. (2014) who showed many pelagic fish species moving vertically in response to hypoxic conditions.
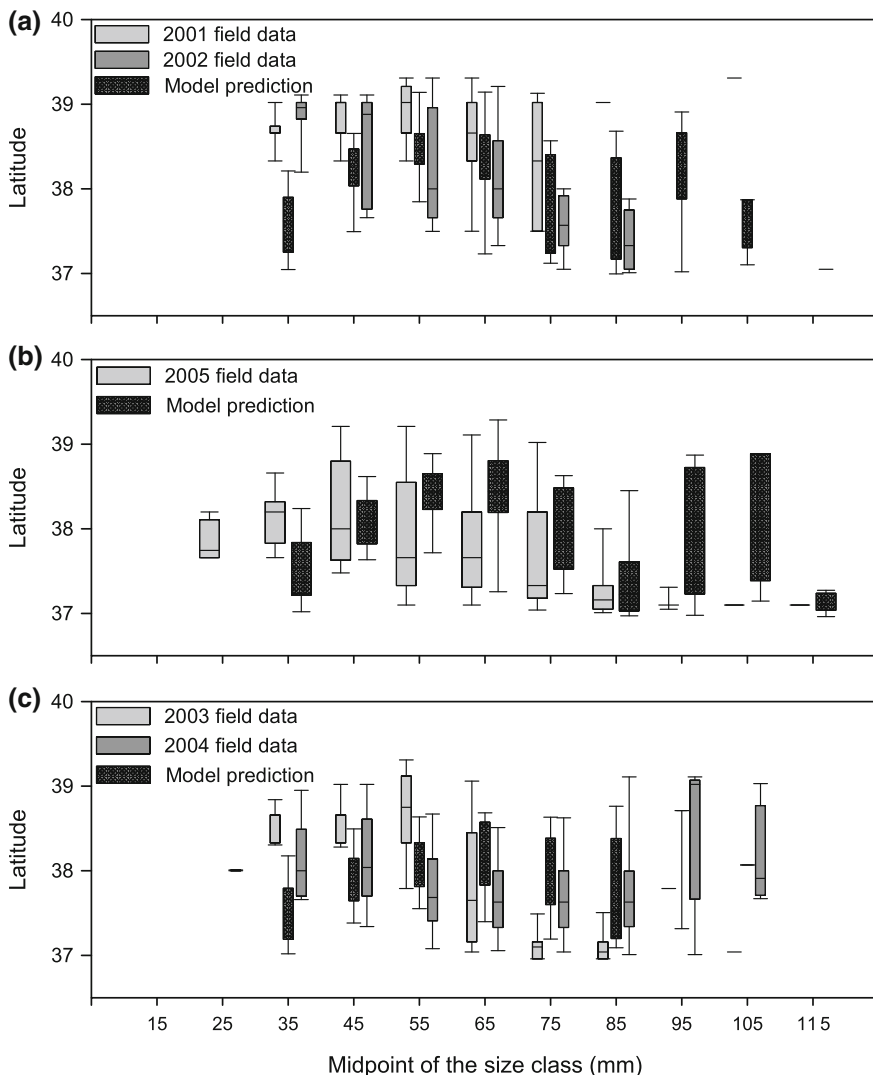
Fig. 12.4 Predicted latitudes (°N) of age 1 and older anchovy in October for the last 3 years water year types: (dry (**a**), normal (**b**), wet (**c**)) of the baseline simulation under high recruitment compared to field observations of the distributions of anchovy in the fall. Years of the field data were matched to the simulated years based on being dry, normal, or wet water years. Anchovy field distributions are from the CHESFIMS project

12.4.3   Effects of Water Year and Nutrient Loadings on Salinity, Temperature, and Zooplankton

Salinity and water temperature were only affected by water years, while meso-zooplankton was affected by both water years and nutrient loadings scenarios. For salinity, going from dry years to wet years resulted in lower overall salinities and increased the southward extent of low salinity waters (e.g., salinity < 15; Fig. 12.5 top row). Water temperatures were somewhat similar for the dry year and the normal year, but were somewhat cooler in wet years (Fig. 12.5 middle row). Spatially, water temperatures tended to be warmest along the edges of the Bay and in tributaries and coolest along the main channel, particularly in the northern half of the Bay. Mesozooplankton density increased going from dry years to wet years and from decreased nutrient loadings scenarios to increased nutrient loadings scenarios in response to increases in nutrient loadings rates to the Bay (Fig. 12.5 bottom row). Spatially, the main channel of the Bay had the highest mesozooplankton densities, but this is in part a result of the mesozooplankton densities being depth-integrated and the main channel being the deepest portion of the Bay. Microzooplankton (not shown) had similar patterns to mesozooplankton.

The effects of water years and nutrient loadings scenarios on salinity, temperature, zooplankton, and other water quality variables are covered in detail in Cerco and Cole (1993), Cerco et al. (2010), and Cerco and Noel (2013).

12.4.4   Effects of Water Year and Recruitment Level in Baseline Simulations

Recruitment level affected YOY anchovy lengths more than water years (Fig. 12.6). Anchovy in the low recruitment scenario (Run 1) generally reached longer lengths than anchovy in the high recruitment scenario (Run 2) (Fig. 12.6a vs. b). However, there was little difference in the length distributions of anchovies across water years (middle bars for each water year in Fig. 12.6a, b). Similar results were seen for October biomasses (Fig. 12.6c, d) and abundances (Table 12.4) of YOY anchovy, though there was more variability across water years for biomass and abundance than for lengths. Across water years, YOY anchovy biomasses were similar for all three water years under low recruitment (18,393–22,502 metric tonnes), but higher for the normal and wet years than for dry year (about 39,000 vs. 28,346 metric tonnes) under high recruitment (Table 12.4; Fig. 12.6c, d). The same pattern was predicted for YOY abundance—similar for all years under low recruitment (44.4–48.4 $\times$ 10^9 individuals) and higher for the normal and wet years than for the dry year (187.6 and 177.9 vs. 169.1 $\times$ 10^9 individuals) under high recruitment.

Water year had a larger effect on anchovy spatial patterns than recruitment level. As would be expected, anchovy densities (all ages) were generally higher under high recruitment than low recruitment (note scale of color bar in Fig. 12.7). Across
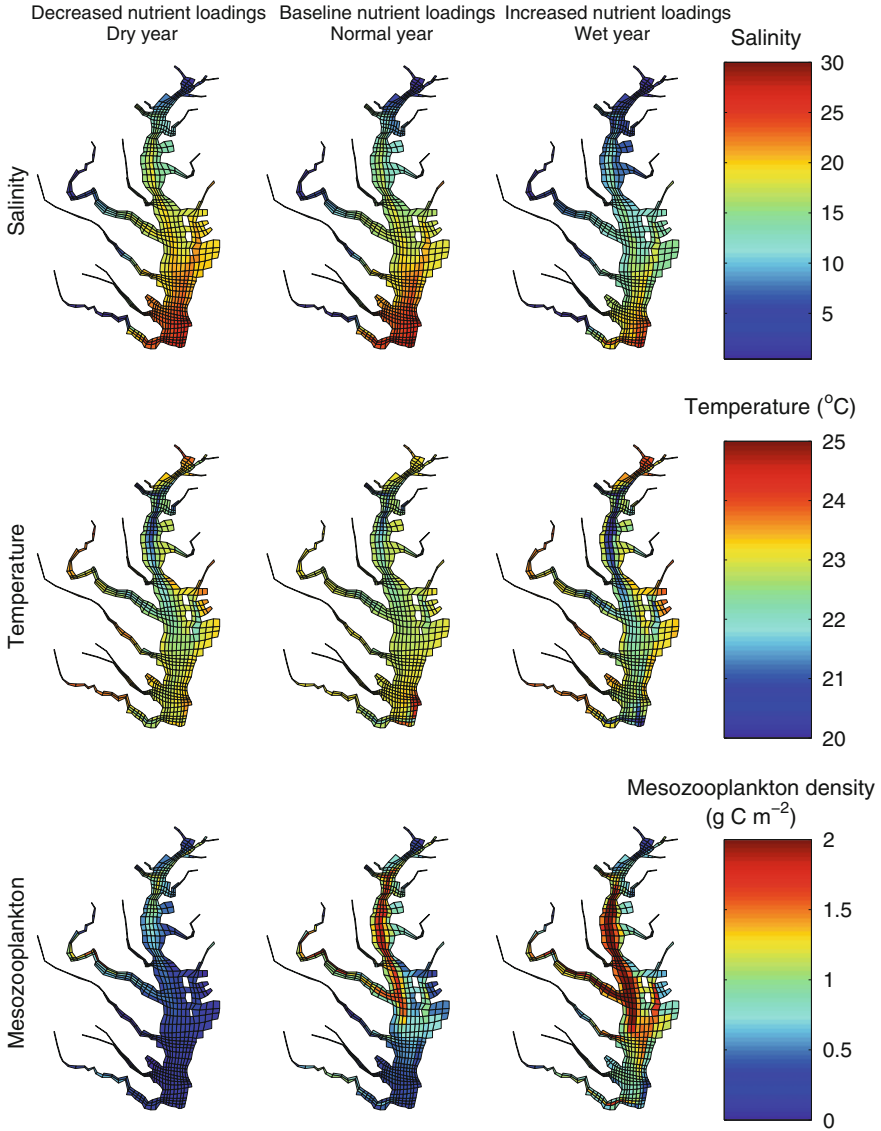
Fig. 12.5 July spatial patterns of depth-integrated salinity (*top row*), temperature (*middle row*), and mesozooplankton densities (*bottom row*) for the dry year of the decreased nutrient loadings scenario, the normal year of the baseline nutrient loadings scenario, and the wet year of the increased nutrient loadings scenario. The three scenarios were selected to show the full range of the nutrient loadings scenarios (e.g., the extreme minimum, "typical," and maximum nutrient loadings scenarios)
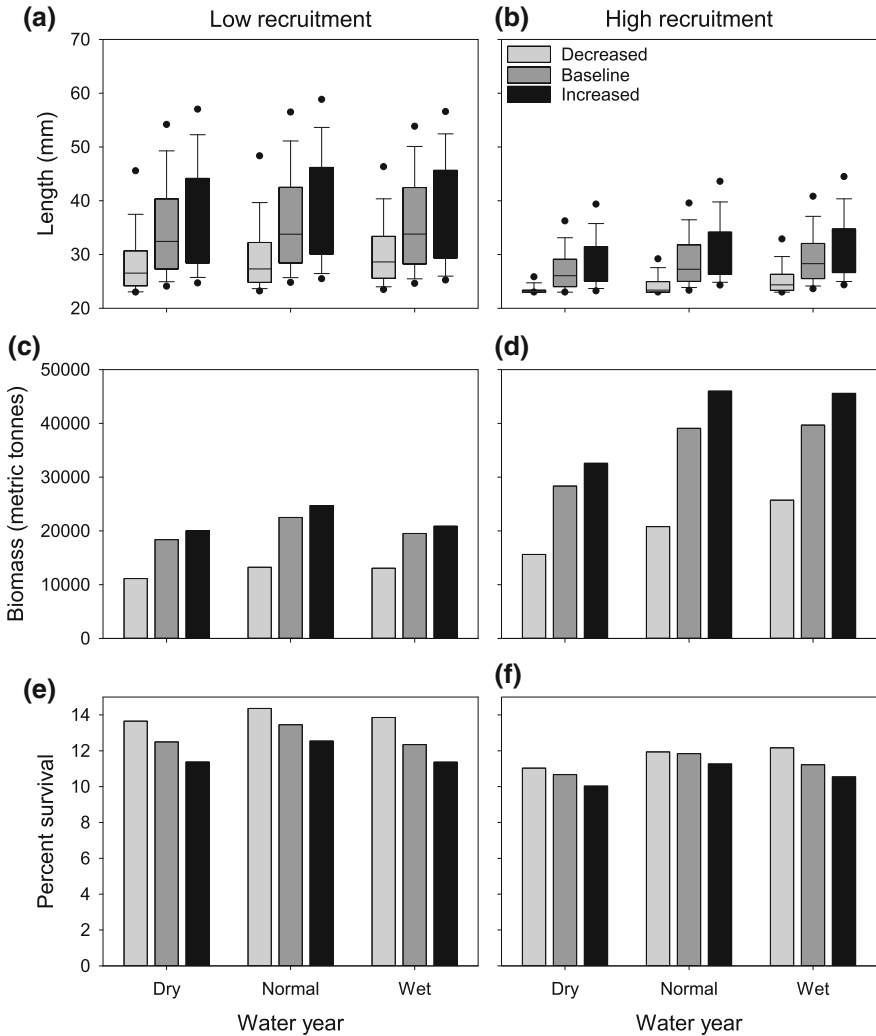
Fig. 12.6 Comparison of YOY bay anchovy October length distributions (**a**, **b**), October biomass (**c**, **d**), and survival from recruitment to October (**e**, **f**) across recruitment levels (*low* and *high*), water year types (dry, normal, and wet), and nutrient loadings (decreased, baseline, and increased). The last 3 years in each simulation were used as dry, normal, and wet year types. For anchovy length *box plots*, *circles* show the 5th and 95th percentiles of the distributions, *whiskers* show the 10th and 90th percentiles, the *box* shows the 25th and 75th percentiles, and the *solid line* in the *box* shows the median

water years, the mean latitude of anchovies in July was farther south in the wet year compared to the normal and dry years, likely in response to changes in the extent of hypoxia between wet and dry years. In the wet year, bottom layer hypoxia extended further south and was more intense than in normal and dry years (not shown). The
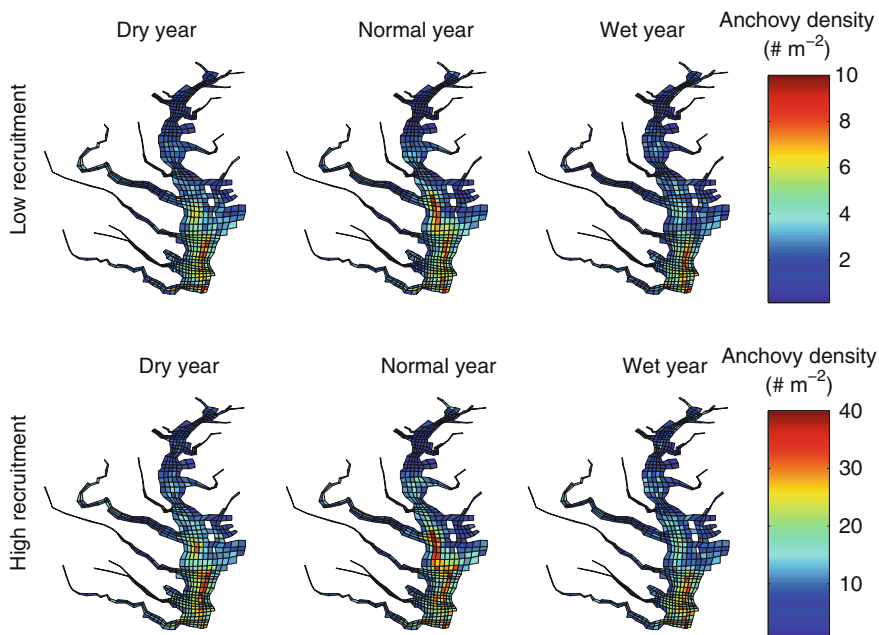
Fig. 12.7 July depth-integrated (# m^{-2}) anchovy densities for the last 3 years (dry, normal, and wet) of the baseline simulation under low recruitment (*top row*) and under high recruitment (*bottom row*). Note the difference in the scale on the *color bars*

effect of water year type on latitude in July was roughly consistent under low and high recruitment levels. Under low recruitment, mean latitude of age-1 and older individuals in July was 37.27°N for the wet year versus 37.35°N and 37.33°N for the dry and normal years. Under high recruitment, mean latitude in July was also lowest (37.33°N) for the wet year compared to the normal and dry years (37.43°N and 37.41°N, respectively).

12.4.5   Effects of Nutrient Loadings

Changing nutrient loadings (Runs 3–6) affected dissolved oxygen concentrations and zooplankton densities in the eutrophication model. Increasing nutrient loads by 50% had a relatively small effect on hypoxic volume (Fig. 12.2). Reducing nutrient loadings had a much larger effect on hypoxic volumes, with a 50% reduction in nutrient loadings resulting in a 20–40% reduction in hypoxic volume (Fig. 12.2). Higher nutrient loadings resulted in higher zooplankton densities throughout the Bay (and vice versa).

Fig. 12.8 Causes of anchovy mortality for all anchovy individuals dying over the course of the 3 prerun years and the 10 water years from 1984 to 1993 for decreased, baseline, and increased nutrient loads and low and high recruitment. Causes of mortality include exposure to low DO (hypoxia), starvation, old age, and general (size-dependent) mortality
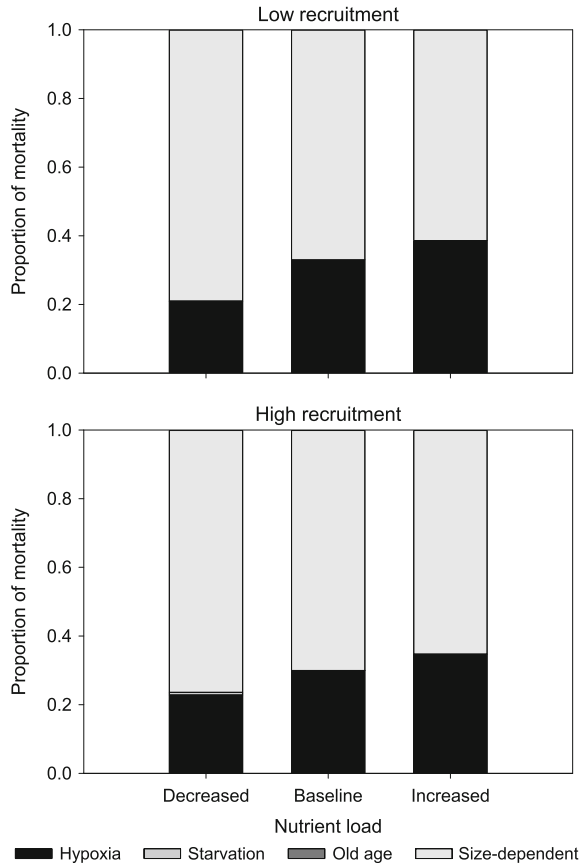
The effects of increasing or decreasing nutrient loads on bay anchovy were consistent across the two recruitment levels and the three water year types. Increased nutrient loadings resulted in increases in YOY anchovy lengths and biomasses, while decreased nutrient loadings resulted in decreases in lengths and biomasses (Fig. 12.6a–d). However, YOY anchovy survival rates were inversely related to nutrient loadings, with increased nutrient loads resulting in lower survival rates for both recruitment levels (Fig. 12.6e, f), primarily due to increases in mortality due to increasing rates of exposure to hypoxic conditions (Fig. 12.8) as the volume of hypoxic water increased (Fig. 12.2). Changes in anchovy survival rates (Fig. 12.6e, f) were small relative to the changes in anchovy lengths (Fig. 12.6a, b), which resulted in increased nutrient loadings producing higher biomasses of YOY bay anchovy (Fig. 12.6c, d) despite the higher YOY mortality rates. We note that going from baseline nutrient loadings to increased nutrient loadings had a smaller effect on anchovy lengths, biomass, and survival than going from baseline to decreased nutrient loadings.

12.4.6   Effects of Additional Hypoxia-Related Mortality

For the low recruitment level (Runs 7–9), reducing recruitment to 86% of the baseline low recruitment level was sufficient to reduce October biomass of YOY anchovy in the increased nutrient loadings scenario to the same level as the biomass obtained under baseline nutrient loadings (Fig. 12.9a). This same reduction in recruitment resulted in the offsetting of the nutrient-fueled increased high biomass for all three water year types. Under high recruitment (Runs 10–12), recruitment had to be reduced to 52% of the baseline high recruitment level to result in October YOY anchovy biomasses that were approximately equal to biomasses under baseline nutrient loadings (Fig. 12.9b).
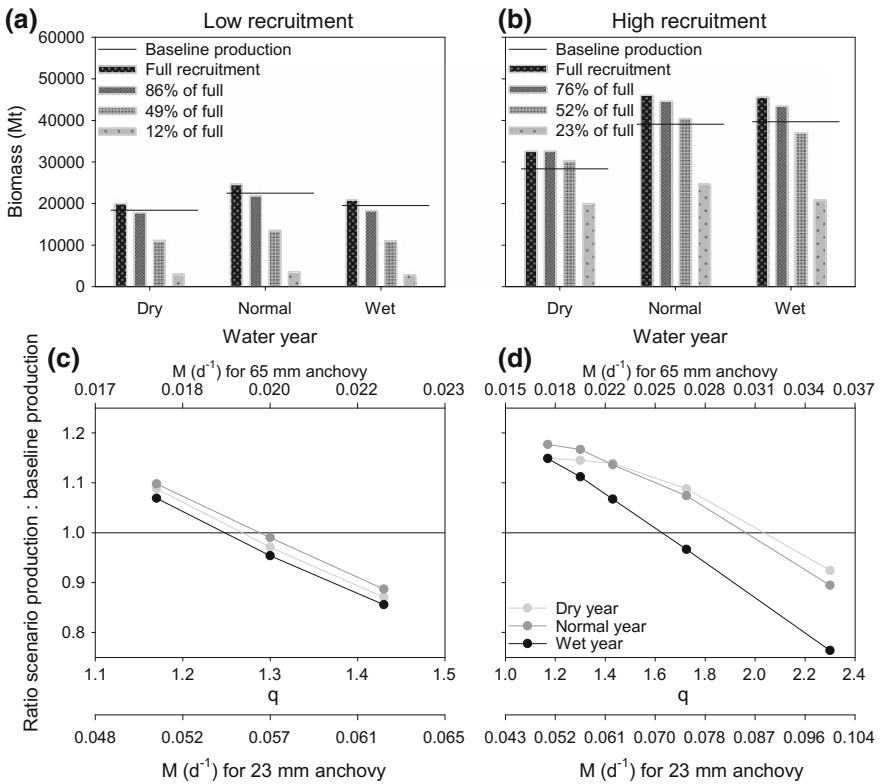
Fig. 12.9 Effects of reduced recruitment (**a**, **b**) and increased juvenile and adult mortality rate (**c**, **d**) under increased nutrient loadings on bay anchovy YOY biomass in October by water year type and for the low and high recruitment levels. The October YOY biomass values for the last three years (dry, normal, and wet) of each simulation were used. Panels **a** and **b** show the October biomass values obtained from simulation; the *horizontal lines* show the biomass for baseline nutrient loadings. Panels **c** and **d** show the ratio of October biomasses (changed q biomass/baseline) for increasing values of q under increased nutrient loadings. In Panels **c** and **d**, the *horizontal line* at 1.0 indicates when the biomasses were the same under increased q and baseline simulations

For the low recruitment level (Runs 13 and 14), increasing q from 1.17 to 1.30 resulted in October YOY anchovy biomass under increased nutrient loadings dropping to the same level as under baseline nutrient loadings (Fig. 12.9c). Increasing q from 1.17 to 1.30 translated into the mortality rate of a 23 mm long individual increasing from 0.05 d^{-1} to 0.057 d^{-1} and for a 65 mm long adult to increase from 0.018 d^{-1} to 0.020 d^{-1}. Much larger increases in q were needed to reduce October YOY biomasses back down to baseline levels under high recruitment (Runs 15–18). During wet years, an increase of q from 1.17 to ~1.6 was needed (black line in Fig. 12.9d), while for normal and dry years q had to increase even more to about 2.0. Increasing q from 1.17 to 1.6 resulted in mortality rate of a 23 mm individual increasing from 0.05 to 0.070 d^{-1} and for a 65 mm individual increasing from 0.018 to 0.025 d^{-1}. A q value of 2.0 resulted in about a 75% increase in mortality rate of juveniles and adults (from 0.05 to 0.087 d^{-1} and from 0.018 to 0.031 d^{-1}).

12.5   Discussion

The effects on anchovy of increased and decreased nutrient loadings depended on the assumptions made about hypoxia causing direct mortality on eggs and larvae and causing increased mortality on juveniles and adults due to assumed changes in anchovy and predator vertical spatial overlap. If we assume that mortality would only be caused by direct exposure of juveniles and adults to hypoxia, then a 50% change in nutrient loadings would have the expected "fertilizer" effect of changing food availability and changes in growth would dominate the response of anchovy. Decreased nutrient loadings would result in smaller YOY anchovy lengths and lower biomass in October, while increased nutrient loadings would result in larger YOY anchovy lengths and slightly higher biomass. These results include low DO effects on juvenile and adult growth and mortality arising from direct exposure to low DO and also reflect avoidance behavior by juveniles and adults of low DO. The simulations ignored DO effects on egg and larval mortality and any mortality changes related to habitat overlap between anchovy and their predators.

However, if we assume that egg or larval mortality (i.e., reduced recruitment to 23 mm) or juvenile and adult mortality are related to the nutrient loadings via hypoxia, then the predicted positive effects on anchovy of increased nutrient loadings can be offset and even reversed by simultaneous changes in hypoxia extent and intensity. Under low recruitment, a 14% reduction in the number of recruits was sufficient to eliminate the benefits of increased nutrient loadings on anchovy biomass, while even larger reductions in recruitment could reduce anchovy biomass to levels that were less than half of those under baseline nutrient loads (Fig. 12.9a). Within the prerecruit phase, an effect on eggs and yolk-sac larvae is more likely than on larvae. Adamack et al. (2012) found that egg mortality was 2-fold to 7-fold higher when nutrient loads were increased, while the response of early larvae was complicated because of shifting degrees of vertical overlap with their invertebrate

predators. Alternatively, juvenile and adult mortality rate would only need to increase from 0.051 d^{-1} to 0.056 d^{-1} for 23 mm anchovy and from 0.018 d^{-1} to 0.020 d^{-1} for 65 mm anchovy due to more spatial overlap with predators to also offset the benefits of increased nutrient loadings (Fig. 12.9c). While the same general result was obtained under high recruitment, larger changes in mortality related to increased nutrient loadings effects were needed.

We carried out some additional model simulations under increased nutrient loadings with both sources of hypoxia-related mortality (direct egg/larval mortality; predation on juveniles and adults due to changes in the degree of vertical spatial overlap) changed simultaneously. While the reductions in recruitment and increased mortality needed to offset increased biomass were reasonable when examined alone for low recruitment, much larger changes were needed under high recruitment. We did not do an exhaustive search of all combinations of reduced recruitment and increased q values that would offset nutrient-fueled higher production under high recruitment; rather, we tried a few combinations. For example, a combination of a 16% increase in juvenile and adult mortality rates combined with a 14% reduction in recruitment in wet years and a 50% reduction in dry years was sufficient to offset the benefits of increased nutrient loadings. Another viable combination was a 22% increase in juvenile and adult mortality rates combined with a 14% reduction in recruitment in wet years and a 25% reduction in dry years.

We also performed some additional simulations to explore the changes in mortality needed to offset the reduced growth predicted under decreased nutrient loadings. Predicted October YOY biomass under low recruitment with decreased nutrient loadings was about 60% of the biomass under low recruitment with baseline nutrient loadings across the 3 year types (Fig. 12.6c). One combination that offsets the reduced biomass under decreased nutrient loadings was assuming that reduced hypoxia spatial extent with decreased nutrient loadings would result in lowered egg and larval mortality and therefore high recruitment (rather than low recruitment) and less overlap of anchovy with their predators and therefore q would decrease from 1.17 to 0.585. Predicted October YOY biomass under decreased nutrient loadings but with these improved conditions was higher than the biomass predicted under baseline loadings for the three water year types. There are other combinations of egg and larval mortality (recruitment) and juvenile and adult mortality (q values) that would also offset the reduced biomass predicted with decreased nutrient loadings.

Thus, the apparent benefit of increased nutrient loadings (and by analogy of decreased loadings) depends on both the increased zooplankton predicted (more food) and possible increased mortality due to the direct and indirect effects hypoxia. Under low recruitment, relatively small reductions in recruitment or increased juvenile and adult mortality, and even smaller effects if both are operating simultaneously, were sufficient to offset or even reverse the effects of changes in nutrient loadings. Larger reductions in recruitment or increased mortality were needed under high recruitment conditions. Relatively large, but not impossible, reductions in mortality due to less hypoxia offset the reduced growth under decreased nutrient loadings. Determining the likelihood and realism of the needed changes in egg to

larva and juvenile and adult mortality rates due to variation in hypoxia will require a combination of field data collection coordinated with modeling in the future.

We included high and low recruitment and different water year types to bound model predictions of responses to changes in nutrient loadings and the associated changes in zooplankton and hypoxia. We used different simulated years to represent dry, normal, and wet year types; however, we used only single years to represent each of these types. In reality, there is also variability among years within dry, normal, and wet year types. Recruitment level had the expected effect on biomass and abundances, with the contrast between low and high recruitment showing the effects of density-dependent growth and survival of YOY. Mean length of YOY in October was almost 50% larger under low recruitment compared to high recruitment. The slowed growth results in consistent, but relatively small, changes in YOY survival from individuals being smaller with a mortality rate that decreased with length (Rose et al. 2001). Wang et al. (1997) and Cowan et al. (1999) also found density-dependent growth and survival using an individual-based anchovy population model configured for a single, well-mixed box for the mesohaline region of Chesapeake Bay. However, Jung and Houde (2004b) hypothesized that anchovy should have higher survival rates during wet years than dry years due to their higher concentrations in a smaller area satiating predators. This potential response of anchovy mortality rates to water years cannot be seen in our simulations, as predators are only included as a general size-dependent mortality term. Our predicted changes in survival were for individuals from recruitment at 23 mm to October; whether the effect would be amplified if the dynamics of the larval stage or predators were simulated is not clear.

Water year type, for a given level of recruitment, had smaller effects on biomass, abundance, and lengths, but did cause a southward movement in wet years (Figs. 12.4 and 12.7). The change in latitudinal distributions is consistent with Jung and Houde (2004b). They suggested that during wet years, anchovy would be located further south as their northward movement would be blocked by low DO in the deeper waters of the mid-Bay region.

The idea that eventually the negative effects of hypoxia associated with increased nutrient loadings result in reduced fish production has been widely discussed. Cross-system comparisons have shown that estuarine systems with higher nutrient loads generally have higher biological production (Caddy 1993, Nixon and Buckley 2002, Breitburg et al. 2009a, b). Caddy (1993) suggested that eutrophication in a coastal ecosystem will initially increase the production of pelagic and demersal fish species, but predicted that further increases in eutrophication would eventually cause the production of demersal fish to decline while pelagic fish production would continue to increase or plateau. Diaz and Rosenberg (2008) offer a similar argument of increasing nutrient loadings eventually leading to a decline in fish populations via hypoxia decreasing benthic energy production that results in decreased consumer production. Often in these reviews (e.g., Breitburg et al. 2009b), the potential for the negative effects of hypoxia from increased nutrient loadings causing a decline in fish populations and fisheries, as suggested by Caddy, is discussed; however, the empirical evidence for the "tipping point" is often limited

with a few case studies offered as possible examples. Our analysis offers a case study using a common pelagic species in Chesapeake Bay and illustrates how coupled biophysical modeling can be used to quantify the negative direct and indirect effects needed to offset the increased production from increasing nutrient loadings. Our results can also be used to quantify the positive direct and indirect effects needed to offset the reduction in production under decreased nutrient loadings scenarios.

Our approach used here was a bottom-up analysis of the population dynamics of a pelagic species. Despite hypoxia being a lower water column phenomenon, there are many examples of analyses of hypoxia effects on pelagic fish species (Vanderploeg et al. 2009; Dylander and Cerco 2010; Pothoven et al. 2012), including studies that specifically dealt with bay anchovy (Ludsin et al. 2009; Adamack et al. 2012; Zhang et al. 2014). Our analysis also focused on how nutrient loadings affected phytoplankton and zooplankton as part of the water quality modeling (i.e., bottom-up), but any other responses of the food web were assumed unaffected by nutrient loadings and associated hypoxia. We did account for prerecruit (egg to larval) mortality and juvenile and adult mortality, but as a sensitivity analysis with forced changes in recruitment and mortality rates and in a non-spatial manner. Increased juvenile and adult mortality would likely have a strong spatial aspect as it would emerge from altered movement of anchovy and their predators (Breitburg et al. 2009b; Ludsin et al. 2009). Other possible responses outside of the population approach are direct and indirect effects on zooplankton (Ludsin et al. 2009; Roman et al. 2012; Elliott et al. 2013); the interplay among zooplankton, ctenophores (*Mnemiopsis leidyi*), and larval fish (Kolesar et al. 2010, 2017); and spatially explicit losses of benthic production (Diaz and Rosenberg 2008). These top-down and food web effects, which were mostly ignored or dealt with by forcing changes in mortality in our model simulations, can modify the predicted anchovy responses to changes in nutrient loadings we obtained here using a population-based approach driven by a hydrodynamics–eutrophication model.

We have successfully demonstrated that we can dynamically couple the three-dimensional Chesapeake Bay water quality model with a population dynamic model of bay anchovy. Most analyses of the relationships among nutrient loadings, hypoxia, and fish have focused on specific life stages (e.g., Adamack et al. 2012), individuals at local scales (e.g., Rose et al. 2009), or changes in habitat (e.g., Constantini et al. 2008). Our approach attempted to operate at the population level for the entire Chesapeake Bay, albeit not full life cycle because we forced recruitment of early juveniles into the model every year. We believe that there are three high-priority expansions needed to the present model. These include continuing to develop the model for bay anchovy in Chesapeake Bay by adding the egg and larval stages as individuals in the simulations, exploring different options for the avoidance behavior, and adding individual predators so they can respond to changes in anchovy distributions and to hypoxia. Making these changes to the model would help us to better understand the effects of changes in nutrient loadings, and concomitant changes in hypoxia, on bay anchovy population dynamics.

References

Adamack AT (2007) Predicting water quality effects on bay anchovy (*Anchoa mitchilli*) growth and production in Chesapeake Bay: linking water quality and individual-based fish models. Dissertation, Louisiana State University

Adamack AT, Rose KA, Breitburg DL et al (2012) Simulating the effect of hypoxia on bay anchovy egg and larval mortality using coupled watershed, water quality, and individual-based predation models. Mar Ecol Prog Ser 445:141–160

Baird D, Ulanowicz RE (1989) The seasonal dynamics of the Chesapeake Bay ecosystem. Ecol Monogr 59:329–364

Batiuk R, Linker L, Cerco C (2013) Featured collection introduction: Chesapeake Bay total maximum daily load development and application. J Am Water Resour Assoc 49:981–985

Boynton WR, Garber JH, Summers R, Kemp WM (1995) Inputs, transformations, and transport of nitrogen and phosphorus in Chesapeake Bay and selected tributaries. Estuaries Coasts 18:285–314

Brandt SB, Mason DM (2003) Effect of nutrient loading on Atlantic menhaden (*Brevoortia tyrannus*) growth rate potential in the Patuxent River. Estuaries 26:298–309

Breitburg DL, Adamack A, Rose KA et al (2003) The pattern and influence of low dissolved oxygen in the Patuxent River, a seasonally hypoxic estuary. Estuaries 26:280–297

Breitburg DL, Craig JK, Fulford RS et al (2009a) Nutrient enrichment and fisheries exploitation: interactive effects on estuarine living resources and their management. Hydrobiologia 629:31–47

Breitburg DL, Hondorp DW, Davias LA et al (2009b) Hypoxia, nitrogen and fisheries: integrating effects across local and global landscapes. Annu Rev Mar Sci 1:329–349

Burkadt J (2014) Geometry—geometric calculations. http://people.scs.fsu.edu/~burkardt/cpp_src/geometry/geometry.html. Accessed 8 Aug 2014

Burton DT, Richardson LB, Moore CJ (1980) Effect of oxygen reduction rate and constant low dissolved oxygen concentrations on two estuarine fish. T Am Fish Soc 109:552–557

Caddy JF (1993) Toward a comparative evaluation of human impacts on fishery ecosystems of enclosed and semi-enclosed seas. Rev Fish Sci 1:57–95

Cerco C, Cole T (1993) Three-dimensional eutrophication model of Chesapeake Bay. J Environ Eng-ASCE 119:1006–1025

Cerco C, Kim S-C, Noel M (2010) The 2010 Chesapeake Bay eutrophication model. A report to the US Environmental Protection Agency Chesapeake Bay Program and to the US Army Engineer Baltimore District. http://www.chesapeakebay.net/content/publications/cbp_55318.pdf. Accessed 23 July 2014

Cerco C, Noel M (2007) Can oyster restoration reverse cultural eutrophication in Chesapeake Bay? Estuar Coast 30:331–343

Cerco C, Noel M (2010) Monitoring, modeling, and management impacts of bivalve filter feeders in the oligohaline and tidal fresh regions of the Chesapeake Bay system. Ecol Model 221:1054–1064

Cerco CF, Noel MR (2013) Twenty-one-year simulation of Chesapeake Bay water quality using the CE-QUAL-ICM eutrophication model. J Am Water Resour Assoc 49:1119–1133

Chesapeake Bay Program (2013) Chesapeake Bay Program http://www.chesapeakebay.net. Accessed 15 Dec 2013

Chesney EJ, Houde ED (1989) Laboratory studies on the effect of hypoxic waters on the survival of eggs and yolk-sac larvae of the bay anchovy, Anchoa mitchilli. In: Houde ED, Chesney EJ, Newberger TA et al (eds) Population biology of bay anchovy in mid-Chesapeake Bay. Solomons, Maryland, pp 98–107

Christensen V, Walters CJ (2004) Ecopath with Ecosim: methods, capabilities and limitations. Ecol Model 172:109–139

Cloern JE (2001) Our evolving conceptual model for the coastal eutrophication problem. Mar Ecol Prog Ser 210:223–253

Conley DJ, Paerl NW, Howarth RW et al (2009) Controlling eutrophication: nitrogen and phosphorus. Science 323:1014–1015

Cooper SR, Brush GS (1991) Long-term history of Chesapeake Bay anoxia. Science 254:992–996

Costantini M, Ludsin SA, Mason DM et al (2008) Effect of hypoxia on habitat quality of striped bass (Morone saxatilis) in Chesapeake Bay. Can J Fish Aquat Sci 65:989–1002

Cowan JH Jr, Rose KA, Houde ED et al (1999) Modeling effects of increased larval mortality on bay anchovy population dynamics in the mesohaline Chesapeake Bay: evidence for compensatory reserve. Mar Ecol Prog Ser 185:133–146

Cronin TM, Vann CD (2003) The sedimentary record of climatic and anthropogenic influence on the Patuxent estuary and Chesapeake Bay ecosystems. Estuaries 26:169–209

Dalyander P, Cerco C (2010) Integration of a fish bioenergetics model into a spatially explicit water quality model: application to menhaden in Chesapeake Bay. Ecol Model 221:1922–1933

Diaz RJ, Rosenberg R (2008) Spreading dead zones and consequences for marine ecosystems. Science 321:926–929

Di Toro D (2001) Sediment flux modeling. Wiley, New York

Dortch MS, Chapman RS, Abt SR (1992) Application of three dimensional Lagrangian residual transport. J Hydraul Eng-ASCE 118:831–848

Elliott DT, Pierson JJ, Roman MR (2013) Copepods and hypoxia in Chesapeake Bay: abundance, vertical position and non-predatory mortality. J Plankton Res 35:1027–1034

Fisher TR, Hagy JD III, Boynton WR et al (2006) Cultural eutrophication in the Choptank and Patuxent estuaries of Chesapeake Bay. Limnol Oceanogr 51:435–447

Gray A (2013) Chesapeake Bay Fiscal 2014 budget overview. Department of Legislative Services, Office of Policy Analysis, Annapolis MD

Hagy JD, Boynton WR, Keefe CW et al (2004) Hypoxia in Chesapeake Bay, 1950-2001: long-term change in relation to nutrient loading and river flow. Estuaries 27:634–658

Hartman KJ, Brandt SB (1995) Trophic resource partitioning, diets and growth of sympatric estuarine predators. T Am Fish Soc 124:520–537

Houde ED, Chesney EJ, Newberger TA et al (1989) Population biology of bay anchovy in mid-Chesapeake Bay. Solomons, Maryland

Houde ED, Zastrow CE (1991) Bay anchovy. In: Funderburk SL, Mihursky JA, Jordan SJ et al (eds) Habitat requirements for Chesapeake Bay living resources, 2nd edn. Living Resources Subcommittee, Chesapeake Bay Program. Annapolis, Maryland, pp 8-1–8-14

Humston R, Ault JS, Lutcavage M et al (2000) Schooling and migration of large pelagic fishes relative to environmental cues. Fish Oceanogr 9:136–146

Humston R (2001) Development of movement models to assess the spatial dynamics of marine fish populations. Dissertation, University of Miami

Johnson BH, Kim KW, Heath RE et al (1993) Validation of three-dimensional hydrodynamic model of Chesapeake Bay. J Hydraul Eng-ASCE 119:2–20

Jung S, Houde ED (2003) Spatial and temporal variabilities of pelagic fish community structure and distribution in Chesapeake Bay, USA. Estuar Coast Shelf S 58:335–351

Jung S, Houde ED (2004a) Production of bay anchovy *Anchoa mitchilli* in Chesapeake Bay: application of size-based theory. Mar Ecol Prog Ser 281:217–232

Jung S, Houde ED (2004b) Recruitment and spawning-stock biomass distribution of bay anchovy (*Anchoa mitchilli*) in Chesapeake Bay. Fish B NOAA 102:63–77

Kemp WM, Boynton WR, Adolf JE et al (2005) Eutrophication of Chesapeake Bay: Historical trends and ecological interactions. Mar Ecol Prog Ser 303:1–29

Kim S-C (2013) Evaluation of a three-dimensional hydrodynamic model applied to Chesapeake Bay through long-term simulation of transport processes. J Am Water Resour Assoc 49:1078–1090

Kolesar SE, Breitburg DL, Purcell JE et al (2010) Effects of hypoxia on Mnemiopsis leidyi, ichthyoplankton and copepods: clearance rates and vertical habitat overlap. Mar Ecol Prog Ser 411:173–188

Kolesar SE, Rose KA, Breitburg DL (2017). Hypoxia effects within an intraguild predation food web of *Mnemiopsis leidyi* ctenophores, larval fish, and copepods. In: Justice D (ed) Modeling coastal hypoxia. Springer, Cham

Lett C, Rose KA, Megrey BA (2009) Biophysical models fish. In: Checkley D, Alheit J, Oozeki Y, Roy C (eds) Climate change and small pelagic fish. Cambridge University Press p 88–111

Ludsin SA, Zhang X, Brandt SB et al (2009) Hypoxia-avoidance by planktivorous fish in Chesapeake Bay: implications for food web interactions and fish recruitment. J Exp Mar Biol Ecol 381:S121–S131

Luo J, Brandt SB (1993) Bay anchovy *Anchoa mitchilli* production and consumption in mid-Chesapeake Bay based on a bioenergetics model and acoustic measures of fish abundance. Mar Ecol-Prog Ser 98:223–236

Luo J, Hartman KJ, Brandt SB et al (2001) A spatially-explicit approach for estimating carrying capacity: an application for the Atlantic menhaden (*Brevoortia tyrannus*) in Chesapeake Bay. Estuaries 24:545–556

Luo J, Musick JA (1991) Reproductive biology of the bay anchovy in Chesapeake Bay. T Am Fish Soc 120:701–710

Magnien RE (1987) Monitoring for management actions: Maryland Office of Environmental Programs Chesapeake Bay Water Quality Monitoring Program, First biennial report. Maryland Office of Environmental Programs, 61 pp

Maryland Department of Natural Resources, Annapolis (2017) Juvenile striped bass survey. http://dnr2.maryland.gov/fisheries/Pages/striped-bass/juvenile-index.aspx. Accessed 3 March 2017

Mauchline J (1998) The biology of calanoid copepods. Adv Mar Biol 33

Miller TJ, Nye JA, Loewensteiner DL (2008) Development and implementation of the Chesapeake Bay Fishery-Independent Multispecies Survey (CHESFIMS)—final report. Technical report series No TS-545-08-020 of the University of Maryland Center for Environmental Science, Solomons, Maryland

Morin LG, Houde ED (1989) Hatch-date frequencies and young-of-the-year growth rates of bay anchovy in mid-Chesapeake Bay. In: Houde ED, Chesney EJ, Newberger TA et al (eds) Population biology of bay anchovy in mid-Chesapeake Bay, Solomons, Maryland, pp 98–107

Newberger TA, Houde ED, Chesney EJ (1989) Relative abundance, age, growth and mortality of bay anchovy (*Anchoa mitchilli*) in the mid-Chesapeake Bay. In: Houde ED, Chesney EJ, Newberger TA et al (eds) Population biology of bay anchovy in mid-Chesapeake Bay. Solomons, Maryland, pp 17–77

Nixon SE, Buckley BA (2002) "A strikingly rich zone"—nutrient enrichment and secondary production in coastal marine ecosystems. Estuaries 25:782–796

Pothoven SA, Vanderploeg HA, Höök TO et al (2012) Hypoxia modifies planktivore–zooplankton interactions in Lake Erie. Can J Fish Aquat Sci 69:2018–2028

Rabalais NN, Turner RE, Dortch Q et al (2002) Nutrient-enhanced productivity in the northern Gulf of Mexico: past, present and future. Hydrobiologia 475:39–63

Roman MR, Pierson JJ, Kimmel DG et al (2012) Impacts of hypoxia on zooplankton spatial distributions in the northern Gulf of Mexico. Estuar Coast 35:1261–1269

Rose KA, Cowan JH Jr, Clark ME et al (1999) An individual-based model of bay anchovy population dynamics in the mesohaline region of Chesapeake Bay. Mar Ecol Prog Ser 185:113–132

Rose KA, Cowan JH Jr, Winemiller KO et al (2001) Compensatory density dependence in fish populations: importance, controversy, understanding and prognosis. Fish Fish 2:293–327

Rose KA, Adamack AT, Murphy CA et al (2009) Does hypoxia have population-level effects on coastal fish? Musings from the virtual world. J Exp Mar Biol Ecol 381:S188–S203

Rose KA, Justic D, Fennel K, Hetland R (2017) Numerical modeling of hypoxia and its effects: synthesis and going forward. In: Justice D (ed) Modeling coastal hypoxia. Springer, Cham

Runge JA, Franks PJS, Gentleman WC et al (2004) Diagnosis and prediction of variability in secondary production and fish recruitment processes: developments in physical-biological modeling. In: Robinson AR, Brink KH (eds) The global coastal ocean: multi-scale interdisciplinary processes, vol 13. The Sea, p 413–473

Scheffer M, Baveco JM, DeAngelis DL et al (1995) Super-individuals a simple solution for modeling large populations on an individual basis. Ecol Model 80:161–170

Snyder JP (1987) Map projections—a working manual. Geological Survey Professional Paper, 1395. U. S. Government Printing Office, Washington, D. C

U.S. Environmental Protection Agency (2010) Chesapeake Bay total maximum daily load for nitrogen, phosphorus and sediment. U.S. Environmental Protection Agency Chesapeake Bay Program Office. http://www.epa.gov/reg3wapd/tmdl/, http://www.epa.gov/reg3wapd/tmdl/ChesapeakeBay/tmdlexec.html. Accessed 16 Dec 2013

U.S Geological Survey (2014) Estimating stream flow entering Chesapeake Bay. http://md.water.usgs.gov/waterdata/chesinflow/. Accessed 11 Aug 2014

Vanderploeg HA, Ludsin SA, Ruberg SA et al (2009) Hypoxia affects spatial distributions and overlap of pelagic fish, zooplankton, and phytoplankton in Lake Erie. J Exp Mar Biol Ecol 381:S92–S107

Wang S-B, Cowan JH Jr, Rose KA et al (1997) Individual-based modeling of recruitment variability and biomass production of bay anchovy in mid-Chesapeake Bay. J Fish Biol 51 (Suppl. A):101–120

Watkins KS, Rose KA (2013) Evaluating the performance of individual-based animal movement models in novel environments. Ecol Model 250:214–234

Zastrow CE, Houde ED, Morin LG (1991) Spawning fecundity, hatch-date frequency and young-of-the-year growth of bay anchovy *Anchoa mitchilli* in mid-Chesapeake Bay. Mar Ecol-Prog Ser 73:161–171

Zhang H, Ludsin SA, Mason DM et al (2009) Hypoxia-driven changes in the behavior and spatial distribution of pelagic fish and mesozooplankton in the northern Gulf of Mexico. J Exp Mar Biol Ecol 381:S80–S91

Zhang H, Mason DM, Stow CA et al (2014) Effects of hypoxia on habitat quality of pelagic planktivorous fishes in the northern Gulf of Mexico. Mar Ecol Prog Ser 505:209–226